An Analysis of Detrusor Dynamics and Urethral Flow in the Canine Urinary Tract, under Obstructive and Non-Obstructive Conditions.

by

Harish S. Lecamwasam

Submitted to the Department of
Mechanical Engineering in Partial Fulfillment of
the Requirements for the
Degree of

MASTER OF SCIENCE
in Mechanical Engineering
at the

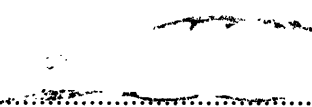Massachusetts Institute of Technology

June 1995

Signature of Author...
Department of Mechanical Engineering
June 9, 1995

Certified by...
Professor Ernest G. Cravalho
Thesis Supervisor

Accepted by...
Professor Ain A. Sonin
Chairman, Graduate School Committee

AN ANALYSIS OF DETRUSOR DYNAMICS AND URETHRAL FLOW IN THE CANINE URINARY TRACT UNDER OBSTRUCTIVE AND NON-OBSTRUCTIVE CONDITIONS

by

HARISH S. LECAMWASAM

Submitted to the Department of Mechanical Engineering on June 9, 1995 in partial fulfillment of the requirements for the Degree of Master of Science in Mechanical Engineering

ABSTRACT

Benign prostatic hyperplasia (BPH) is typically a disease of men aged 40 years, and above. By the age of 50 years, approximately 20% of men are affected, while by the age of 75 years, approximately 75% of men are affected. Given this incidence, and the aging population, BPH has become a major health care issue. The pathology of BPH is induced by a hyperplastic prostate occluding the bladder outlet. How an outlet obstruction impacts both the detrusor function and urethral flow must, therefore, be fully understood before an optimal diagnosis or treatment of BPH can be formulated. This study uses a canine model to evaluate how the passive urethral resistance, the detrusor internal work ($W_{int} = V\Delta p$) and the detrusor external work ($W_{ext} = \int pQdt$) respond to a changing outlet obstruction. The experimental data is also used to define a urethral pressure-area relation, and to characterize urethral flows in terms of a Reynolds number and an entry length.

The detrusor function, outlet resistance and urethral flows of five female canines were assessed under non-obstructive (phase I) and obstructive (phase II) conditions. All urodynamic analyses were performed on a surgically exposed urinary tract. Solid state pressure transducers were used to measure intravesical and distal urethral pressures. An ultrasonic flowmeter was used to obtain an instantaneous measurement of the urethral flowrate. An electrical stimulation (30V, 50Hz, 0.1msec and 10sec duration) of the pelvic nerves was used to induce bladder contractions. All outlet obstructions were modeled using an inflatable sphincter cuff. During the phase II studies, an outlet was assumed non-obstructed at a 0% cuff volume and completely occluded at a 100% cuff volume.

The mean outlet resistances of the phase I studies ranged between 0.07-1.7 $cmH2Os^2ml^{-2}$. As outlet obstruction was increased, the normalized internal work, normalized external work and normalized outlet resistance (all normalized with respect to the corresponding mean phase I result) remained approximately constant until a threshold cuff volume - 60% for the work parameters, and 75% for the resistance - was exceeded. As obstruction was increased beyond the respective thresholds, the normalized outlet resistance and the normalized internal work increased from their (non-obstructed) unity references to 400 and 4 respectively. The normalized external work decreased from unity

to zero.   At cuff volumes below 60%, the magnitudes of the internal work and the external work remained approximately equal. At volumes exceeding 60%, however, the internal work increased while the external work decreased. The concept of the internal work as an elastic energy that is fully recovered during voiding thus appears valid only at low outlet obstructions. As the normalized resistance was increased from unity to 60, the normalized internal work increased exponentially, while the normalized external work decreased exponentially. At normalized resistances exceeding 100, both normalized work parameters were plateaued at their maximum and minimum values of 4 and 0 respectively. Given this exponential correlation, at low outlet obstructions, the internal and external work appear more sensitive to changes in the outlet obstruction than the outlet resistance.

Under non-obstructive conditions, the peak Reynolds numbers R_e^p and entry length to diameter ratios l_e/D obtained ranged between $500 < R_e^p < 1500$, and $30 < l_e/D < 90$. The non-obstructed urethral diameters D computed ranged between $1.5mm < D < 2.5mm$, while the urethral lengths l used for the urodynamic assessments ranged between $75mm < l < 95mm$. The non-obstructed phase I flows were thus typically laminar entry length flows. The peak Reynolds numbers for the obstructed phase II studies also remained within the boundaries of laminar flow.

To Baba...

Jei Sai Ram !

Table of Contents

1 Introduction

The primary goal of this thesis is to provide new insights into the evaluation of benign prostatic hyperplasia (BPH) and to spur new directions in its management. For this, a canine model will be used to elucidate the physiologic impact of a bladder outlet obstruction, as induced by BPH, on detrusor function, outlet resistance and urethral flows. The reader should keep in mind that although many similarities exist between the human and canine urinary systems, the anatomical and pathological information presented in the subsequent introductory material strictly apply only to humans. If specific information regarding canine anatomy is required, the reader is directed to a canine anatomy text. The analytical methodologies discussed in assessing outlet obstruction are however equally applicable to both humans and canines.

1.1   Overview

Anatomically, the urinary system can be divided into an upper urinary tract composed of the two kidneys and ureters; and a lower urinary tract composed of the urinary bladder and urethra. Functionally, this system is responsible for urine formation, collection, transportation and micturition (the voluntary expulsion of urine via the urethra).
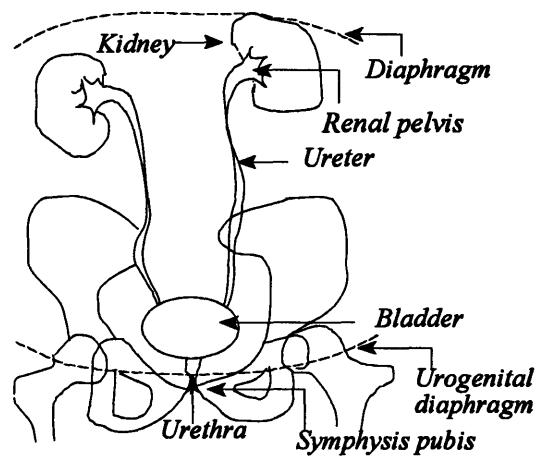

Figure 1.1 An anterior view of the human urinary system.

This thesis is exclusively dedicated to an analysis of the micturitional function of the urinary system. All subsequent discussions and analyses are therefore limited to the lower urinary tract.

1.2   The Lower Urinary Tract

The lower urinary tract is composed of the urinary bladder and the urethra. The bladder is connected to each kidney by a long, muscular ureter, along which filtered urine is propelled by peristalsis. The lower urinary tract can be modeled mechanically as a pump (the bladder), a piping system (the urethra), valves (sphincters), and a nozzle (the external meatus)[1]. Traditionally, the majority of studies investigating voiding function have focused on the urethra. However, during a voiding cycle, the urethra has been shown to play a passive role, only modulating the relation between the bladder pressure and the voiding flowrate. Conversely, voiding patterns under normal and obstructive conditions are dominated by the dynamics of a bladder contraction and its adaptations to varying outflow conditions. Thus, an appreciation of the bladder's role within a voiding cycle is pivotal to the proper understanding of both the physiology and the pathophysiology of micturition.

1.2.1   The Urinary Bladder

The bladder is a hollow, muscular sac that functions as a passive reservoir for urine. An empty adult bladder has an internal diameter of approximately 5cm. It lies retroperitoneally, and is positioned posterior to the pubic symphysis. Anatomically, a bladder can be divided into a dome, a base, and a neck. The dome, in turn, can be divided into an apex, a superior surface, and two anterolateral surfaces. The bladder neck lies most inferiorly, and is connected to the urethra. During filling, the bladder dome rises into the pelvic cavity, while the position of the bladder neck remains approximately stationary. The maximum capacity of a normal adult bladder ranges between 300-500ml.

The bladder contractile tissue can be divided into the detrusor and trigone musculature. Both are comprised of smooth muscle and demonstrate the slow response and fatigue rates characteristic of all smooth muscles. Their physiology is however unique in that conscious control of a bladder contraction, i.e. of micturition, can be learned.

The detrusor refers to the smooth musculature extending over the bladder dome. Around the region of the bladder outlet, the detrusor consists of distinct inner, middle, and outer muscular coats. The inner and outer layers are composed of longitudinal fibers. The former extends over the bladder outlet and into the urethra, while the latter forms an almost complete sheet of circumferentially oriented muscle bundles above the level of the internal meatus. The middle layer consists of circularly oriented muscle bundles that sweep outward along the sides of the bladder from the bladder neck. Despite their circular orientation, these fibers do not provide any sphincteric action. In the remaining regions of the dome, muscles bundles cross each other freely with no definite orientation. Any layering in these regions is thus unclear.

The trigone is a triangular shaped muscle layer, extending over the bladder base between the ureterovesicle junction, and the lip of the internal meatus. It consists of two layers: the superficial layer, and the deep layer. Muscle bundles from the superficial layer pass over the internal meatal lip, and into the proximal urethra. The deep layer forms a dense sheet at the bladder base, and anchors the ureterotrigonal unit. The muscle cells of this layer are largely indistinguishable from those of the detrusor muscle proper.

The bladder is well innervated by the autonomic nervous system. The sympathetic supply via the hypogastric nerves originates at the thoracic and lumbar segments T11-T12, and L1-L2. The parasympathetic supply originates at the sacral segments S2-S4 (the pelvic splanchnic nerves). The primary motor nerve supply to the detrusor and the bladder base (including the trigone) is parasympathetic, and sympathetic respectively.

The bladder vasculature is derived from branches of the internal illiac artery and veins. The interior of the bladder is lined with a transitional epithelium.
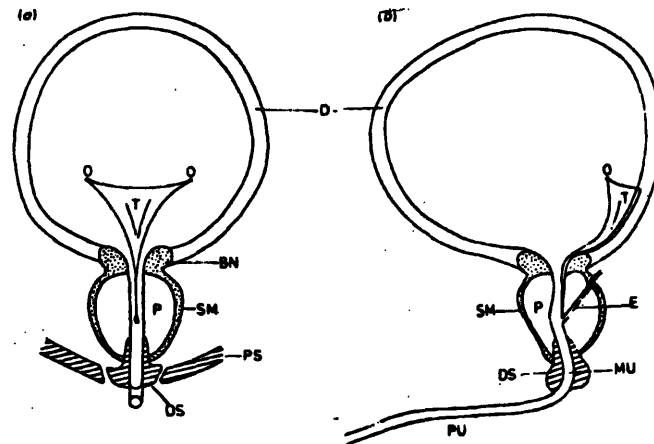
Figure 1.2 Schematic diagram of sections through the male bladder and urethra, viewed (a) from the front, and (b) from the left side. D, detrusor smooth muscle; T, tigone; SM, urethral smooth muscle; DS, distal intrinsic urethral sphincter; PS, periurethral sphincter; BN, bladder neck; P, prostate gland; MU, membranous urethra; PU, penile urethra; EM, external meatus; E, ejaculatory duct; O, ureteral orifices. (After Gosling 1979). From: *Urodynamics, The Mechanics and Hydrodynamics of the Lower Urinary Tract*, Griffiths, D.J., Adam Hilger Ltd, 1980, p 7.

1.2.3   The Urethra

The urethra is a muscular tube connecting the bladder to the external environment, and extends between the bladder outlet and the external meatus. The urethral musculature and epithelial lining are continuous with that of the bladder. At zero flow, the urethra is collapsed, and completely dry. The collapsed walls create a slit-like cross sectional area. The open regions of this cross section are filled with a viscous fluid secreted by the urethral lining, creating a watertight seal. During micturition, the urethra opens to a

maximum diameter of approximately 3 mm. The exact diameter of the urethral lumen at any given location depends upon the local distensibility and static pressure, both of which change along the urethral length.

The striated sphincter urethrae muscle encircles the urethra to form an external voluntary sphincter (refer figure 1.2) at the level of the urogential diaphragm. In the male this sphincter is positioned around the membranous urethra, and in the female, around the mid-urethral segment. In both sexes, the urethra is innervated by the same autonomous nervous supply as the bladder. The external striated sphincter is innervated by the pudendal nerve (S2,3,4) originating from the sacral plexus.

The male and female urethras demonstrate some structural and functional dissimilarities, and are briefly discussed below.

1.2.3.1   The Male Urethra

The male urethra functions as a conduit for both the urinary and the genital systems. The external meatus is positioned at the tip of the glans penis. On average, an adult male urethra is approximately 20 cm in length.

The male urethra can be divided into a prostatic, membranous, and penile region. The prostatic segment is about 3 cm in length. It is surrounded by the prostate gland and contains openings for the ejaculatory ducts. (The circularly oriented muscle bundles of a pre-prostatic region helps prevent any back flow of ejaculate into the bladder.) The membranous urethra is the thickest, least distensible segment, and is about 2.5 cm in length. It involves both striated musculature - the external sphincter - and smooth musculature. The former is oriented in a ring shaped structure, extending between the prostatic apex and the penile bulb. The penile urethra is the longest segment (about 15 cm in length), and is contained within the corpus spongiosum. The most proximal part of this segment is the widest urethral region, and is surrounded by the penile bulb. At its

terminus - the external meatus - the penile urethra narrows to open into the environment. This is the narrowest region of the urethra.
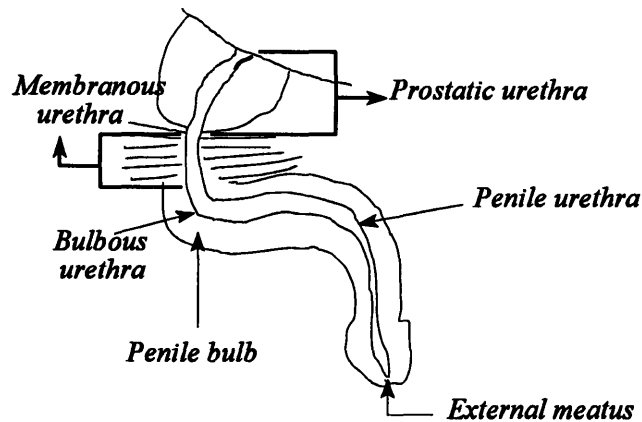
Figure 1.3 Schematic of male urethra. From *Campbells Urology, Anatomy of the Lower Urinary Tract*, Tanagho, E.A., p 53.

1.2.3.2   The Female Urethra

The adult female urethra is about 4 cm in length, 6 mm in diameter, and is a conduit only for urinary flow. It is positioned along the anterior vaginal wall, with the external meatus lying within the vaginal vestibule about 2.5 cm posterior to the glans clitoris. A glandular structure homologous to the male prostate can be seen along the distal end of the female urethra. Although this structure is called the female prostate, it does not acquire the functional or structural complexity of the male prostate. The entire female urethral length is rich in elastin and collagen fibers, and is more distensible than the male urethra.

1.3   Micturition

Micturition, or voiding, is defined as the intermittent, voluntary expulsion of urine from the bladder. The elastic and viscoelastic properties of a bladder allow it to accumulate urine with a minimal rise in bladder pressure during filling. Normally, the bladder fills at a rate of about 1 ml/min. During filling, motor impulses from the sympathetic system prevent any leakage into the urethra by both maintaining a closed urethra (by stimulating a urethral muscle contraction) and inhibiting a bladder contraction. As filling progresses, a sensation of "fullness" will originate from stretch receptors in the bladder wall. If necessary, this urge to void can be ignored up to a critical threshold. Beyond that, a voiding detrusor contraction will begin.

A voiding bladder contraction is caused by the activity of efferent postganglionic parasympathetic nerves. Voiding itself is accomplished by a contraction of the bladder musculature in conjunction with a relaxation of the urethral musculature.

Mechanically, a bladder contraction is represented by a rise in bladder pressure, while a urethral relaxation is represented by a drop in urethral pressure and vice versa. The urethra, which remains in a collapsed state during bladder filling, will open only when the bladder pressure exceeds a minimum urethral opening pressure[i]. Once voiding is complete, the bladder pressure will gradually decrease. As the pressure falls below a critical closure pressure, the urethra will return to its collapsed state starting from its distal regions and continuing proximally up to the bladder neck. The critical urethral opening and closing pressures are not necessarily identical.

During a bladder contraction, motor impulses from the parasympathetic system

---

[i]   Because of its shorter length, a lower resistance is associated with the female urethral than the male urethra. The minimum urethral opening pressure for the female is thus lower than for the male.

will inhibit any urethral muscular contraction. These efferent nerves, along with the afferent nerves conveying information about the bladder state, constitute a micturitional loop. The contraction of the bladder with the simultaneous relaxation of the urethra is termed the micturition reflex. Voluntary control of micturition (within limits) becomes possible once control of the spinal center co-ordinating this reflex is learned.

1.3.1   The Mechanics of Micturition

Micturition is a process under neuromuscular control, and results from an interplay between the expulsive action of the bladder, and the impedance offered to flow by the urethra (refer Figure 1.4). The former can be represented by the pressure of urine within the bladder, the intravesical pressure (p_{ves}). p_{ves} is composed of an intrinsic detrusor component p_{det} (the detrusor pressure), and an extrinsic abdominal component p_{abd} (the abdominal pressure).

$$p_{ves}(t) = p_{abd}(t) + p_{det}(t) \qquad (1)$$

In general, p_{ves} is determined predominantly by p_{det}. The mechanical properties of the bladder are thus governed by the detrusor. In all subsequent discussions, the detrusor and intra-vesical pressures will therefore be considered synonymous.

The detrusor pressure itself arises primarily from the active contraction of the detrusor muscle (and to a lesser extent from the viscoelastic properties of the bladder wall and muscle tone). At any given instant, p_{det} depends upon: (a) the intrinsic strength of the detrusor muscle (b) the level of (parasympathetic) neural stimulation (c) the volume of urine in the bladder, and (d) the outflow rate of urine from the bladder $(Q(t))$.
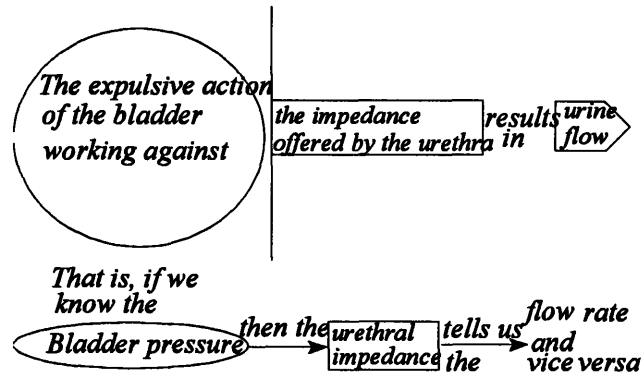
Figure 1.4   Meaning of urethral impedance (From Griffiths, D.J., Mechanics of Micturition. *Neurology and Urodynamics.* p 96, 1988[2])

As with any other muscle, the detrusor, when stimulated, can either shorten or develop force. This compromise between the velocity of shortening (related to the urine flow rate) and the force developed (related to the detrusor pressure) can be depicted using a trade-off curve.

Figure 1.5   Pressure-flowrate trade-off curve for a contracting detrusor.

As can be seen, the same detrusor contraction will produce vastly different detrusor pressures in individuals afflicted with different conditions (e.g. the same detrusor contraction will produce a large p_{det} in obstructed individuals, and a small p_{det} in individuals with low impedance)[ii].

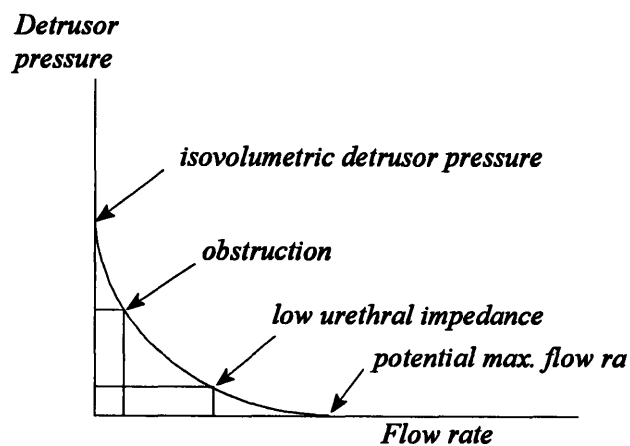Urine from the bladder will enter the urethra only after a critical value of p_{det} has been attained. This is because the urethra provides a finite impedance to the bladder output. A high impedance (low Q for high p_{det}) implies obstruction. Low impedance (high Q for low p_{det}) implies no obstruction. Two alternate approaches can be used to describe this concept of urethral impedance.

1.3.1.1   Energy approach

This approach describes micturition as follows: The detrusor pressure, at a given bladder volume, is a potential energy source for driving flow through a urethra. As flow occurs, a fraction of this potential energy will be dissipated by viscous and inertial effects, while the remainder will appear as the kinetic energy of the exit stream[2] (strictly speaking, it will appear as the *time integral* of the kinetic energy of the exit stream, as will be shown below).

A finite control volume approach can be used to apply the fundamental laws of mechanics and thermodynamics to a finite region of space containing a finite amount of fluid (i.e. a control volume), and explicitly derive the relation between the detrusor pressure (or, alternately, the flow work[iii]) and the flow kinetic energy. The following derivation assumes a basic understanding of control volume theory. An in-depth

---

[ii]   Any p_{det} measurement corresponding to non-zero flow rates alone is thus an inadequate estimate of detrusor contractility. The detrusor pressure at zero flow, the isometric (or isovolumetric) detrusor pressure, is a better indicator of contractility. However, since it is invalid during the period of voiding proper, the usefulness of the isovolumetric pressure is also limited.

[iii]   Defined as the product of the detrusor pressure and the change in bladder volume.

discussion of control volumes and their applications, if required, is available in

Engineering Thermodynamics, Smith, J.L, Cravalho, E.G. pp 350 - 358.
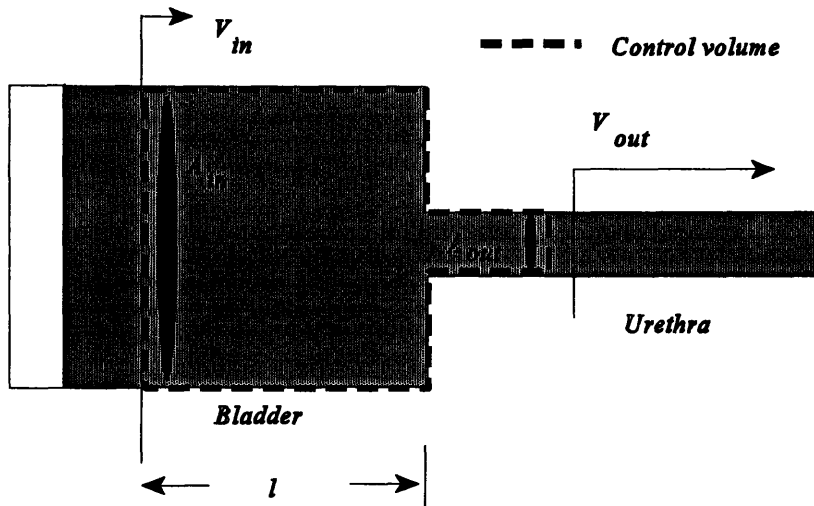
Figure 1.6   The control volume used to derive the relation between the detrusor pressure (or, equivalently, the flow work) and the flow kinetic energy. The bladder and urethra are indicated by the thin line. The thick-dashed line is used to demarcate the borders of a fixed control volume enclosing a fixed mass of fluid.

As shown in Figure 1.6, a system containing a constant mass of fluid (urine) can be defined within a fixed control volume located within the bladder, and extending into the urethra. The first law of thermodynamics states that the rate of change of a system's intrinsic energy (dE_{system}/dt) is equal to the net rate of energy transfer to the system by heat ($\delta H/dt$) and work ($\delta W/dt$). Mathematically, this can be expressed as:

$$\frac{dE_{system}}{dt} = \frac{\delta H}{dt} - \frac{\delta W}{dt} \qquad (2)$$

Here, the sign convention adopted implies that heat added to a system is positive, and work done on the system is negative. This basic expression can be extended to yield the following first law of thermodynamics for a control volume[3]:

$$\frac{dE}{dt} = \frac{\delta H}{dt} - \frac{\delta W_{shear}}{dt} + \sum \frac{dm}{dt}(h + \frac{v^2}{2} + gz)_{inflow} + \sum \frac{dm}{dt}(h + \frac{v^2}{2} + gz)_{outflow} \qquad (3)$$

Where, dm/dt represents the rate of mass inflow/outflow, h the property enthalpy, v the velocity of fluid at the inflow/outflow ports, g the gravitational acceleration, and z the elevation from some arbitrary reference. The two summation terms in equation (3) have been added to the basic first law expression (equation (2)) to account for the net energy convected to the system by bulk flow across the control surface. The work represented by the $\delta W_{shear}/dt$ term in equation (3) represents the shear work transfer, and includes all work transfers for the system *except* those resulting from a pressure and normal displacement of the system boundary (i.e. pdV work transfers). All of this pdV work transfer is accounted for in the enthalpy h, defined in terms of a specific internal energy u, fluid pressure p and fluid density ρ.

$$h = \frac{p}{\rho} + u \qquad (4)$$

Since the control volume defined in Figure 1.6 is fixed, all unsteady effects can be neglected. Further, since a control volume containing a constant fluid mass is defined, the rate of energy change within the control volume is zero (i.e. within a fixed system, energy can neither be created nor destroyed). It should be noted that since the length l of the control volume within the bladder can be made infinitesimally small (without invalidating the following derivation), the assumption of a system of constant mass is applicable through the entire voiding cycle. Equation (3) can be simplified as follows:

Since the mass within the control volume is constant for all time, the mass flowrate dm/dt into the control volume will equal the mass flowrate out of the control volume. If the fluid within the bladder is assumed to be incompressible, the flowrate Q will be a

constant through the control volume yielding the following expression for the conservation of mass for the system:

$$\frac{dm}{dt} = \rho Q = c \rightarrow A_{inflow} \cdot v_{inflow} = A_{outflow} \cdot v_{outflow} \qquad \text{and,} \quad v_{inflow} = v_{outflow} \frac{A_{outflow}}{A_{inflow}} \qquad (5)$$

Since, $A_{inflow} \gg A_{outflow}$, v_{inflow} is negligible compared to $v_{outflow}$. Also, since all flow occurs along a horizontal axis for the system in Figure 1.6, the contribution to the first law from changes in elevation are negligible. If a zero heat transfer is also assumed, equation (3) can be re-written as (with $dm/dt = \rho Q$):

$$0 = -\frac{\delta W_{shear}}{dt} + \sum \rho Q (\frac{p}{\rho} + u)_{inflow} - \sum \rho Q (\frac{p}{\rho} + u + \frac{v^2}{2})_{outflow} \qquad (6)$$

Equation (6) can be further simplified by noting that the control volume in Figure 1.6 contains a single inflow and a single outflow port, and that the inflow pressure is simply the detrusor pressure p_{det}, yielding:

$$p_{det} Q = \frac{\delta W_{shear}}{dt} + p_{outflow} Q + \rho \frac{v_{outflow}^2}{2} Q + \rho Q (u_{outflow} - u_{inflow}) \qquad (7)$$

Any kinetic energy dissipated within the system will transform into an increase in the specific internal energy u through the dissipative process. The term $\rho Q (u_{outflow} - u_{inflow})$ in equation (7) should thus reflect any flow kinetic energy dissipated within the urethra by an increase in $u_{outflow}$ relative to u_{inflow}. However, because the coupling of the kinetic and specific internal energies in fluids is weak, the increase in the specific internal energy from any kinetic energy dissipation will be minimal. This allows the approximations $u_{outflow} \approx u_{inflow}$ and, $\rho Q (u_{outflow} - u_{inflow}) \approx 0$. Equation (7) can now be written as,

$$(p_{det} - p_{outflow})Q = \frac{\delta W_{shear}}{dt} + \rho \frac{v_{outflow}^2}{2} Q \qquad (8)$$

Equation (8) is the final expression of the first law of thermodynamics for the system defined in Figure 1.6. Hydrodynamically, the product pQ represent fluidic power (i.e. rate of work done, or energy consumed). However, since the concepts of work and energy (i.e. $\int p dV$ as opposed to its time derivative) are more physiologically relevant, equation (8) is best interpreted by examining its time integral:

$$\int (p_{det} - p_{outflow}) \frac{dV}{dt} dt = \int (p_{det} - p_{outflow}) dV = W_{shear} + \int \rho \frac{v_{outflow}^2}{2} Q dt \qquad (9)$$

Physiologically, equation (9) states that the difference between the detrusor flow work (defined as the integral $\int p dV$) at the inflow and outflow ports is equal to the sum of the shear work transfer and the time integral of the kinetic energy at outflow port (with the kinetic energy represented by $\rho(v_{outlet}^2/2)Q$). The placement of the outflow port as shown in Figure 1.6 is arbitrary. If the intra-urethral arm of the control volume is extended such that it is adjacent to the external meatus, and the subject voids into the atmosphere, $p_{outflow} = p_{atmospheric}$. The difference $p_{det} - p_{outflow}$ thus becomes the gage detrusor pressure (i.e. detrusor pressure measured relative to atmospheric pressure) that is routinely measured using a pressure transducer. The first law expression then effectively reduces to the functional expression of the energy approach:

$$\int p_{det} dV = W_{shear} + \int \rho \frac{v_{es}^2}{2} Q dt = W_{shear} + \int \rho \frac{v_{es}^2}{2} dV \qquad (10)$$

with v_{es} representing the velocity of the exit stream. The time integral of the kinetic energy has also been simplified by noting that $Q = dV/dt$. Figure 1.7 is a graphical representation of this relation as drawn by Griffiths[2].
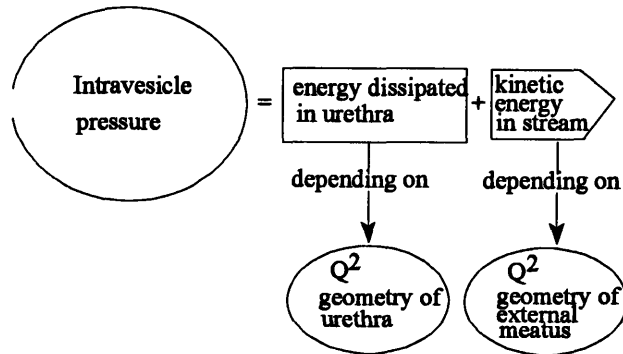
Figure 1.7 Energy balance during voiding according to energy approach. (From Griffiths, D.J. Mechanics of Micturition, *Neurology and Urodynamics.* p 99, 1988)

.

Several issues regarding the correspondence between the functional and graphical forms of equation (10) merit a brief mention. First, it should be noted that Figure 1.7 explicitly considers fluidic losses in the urethra. It thus implies that the term $\rho Q(u_{outflow} - u_{inflow})$ in equation (7) must be considered when computing a urethral energy balance. However, urethral losses have been characterized as minimal[4]. Also, as discussed, the contribution of any urethral losses to the term $\rho Q(u_{outflow} - u_{inflow})$ in equation (7) is negligible. (The reader is reminded that the first law of thermodynamics uses the term $\rho Q(u_{outflow} - u_{inflow})$ to account for any kinetic energy losses in the urethra). Equation (10) will thus still be considered an adequate representation of the urethral energy balance.

Figure 1.7 also essentially ignores any biochemical energy expended by a detrusor when raising intravesical pressure against a closed outlet. (Each voiding contraction proper is preceded by an isometric contraction where the detrusor pressure is increased against a closed urethra with zero volume voided. This will be discussed in detail in section 1.3.1.2). Equation (10) accounts for this non pdV energy transfer with the $\delta W_{shear}/dt$ term. Second, the proportional relation between the kinetic energy, the (flowrate)^2 and geometry of the external meatus as shown in Figure 1.7, although not explicit in equation (10), becomes evident by substituting $Q=vA$, yielding $\frac{1}{2}\int \rho v^2_{es}dV = \frac{1}{2}\int \rho(Q^2/A_{exit}^2)dV$, with

A_{exit} the cross sectional area of the external meatus. Also, according to Figure 1.7 all fluidic losses incurred are proportional to Q^2. This implicitly assumes that flow through the urethra is turbulent, and that losses are predominantly due to inertial effects - with laminar flow, the pressure drop due to frictional losses ΔP is linearly related to the flowrate Q as expressed by Poiseuille's equation. However at high flowrates, the pressure drop is more accurately described by Rhorer's equation: $\Delta P = k_1 Q + k_2 Q^2$, with the Q^2 term indicating the effect of turbulence. When turbulence is present, losses are incurred by eddies and mixing, with the associated pressure drop depending upon the fluid density (as opposed to fluid viscosity, as with Poiseuille flow). The precise characteristics of urethral flows along with the relevant tube laws are treated in detail within the Results section, and will not be discussed further at this juncture.

Hence, given all of the assumptions discussed above, the precise statement of the energy approach to urethral flow is that any difference in the detrusor flow work between a proximal and a distal point along the flow stream, will be equal to the sum of a shear (non pdV) work term and the time integral of the flow kinetic energy evaluated at the distal point (refer equation (9)).

Thus far, attempts to use this information in evaluating outlet resistance have been largely unsatisfactory. Since the distensible tube approach discussed next is extremely powerful in this context, the application of the energy approach to urethral impedance will not be discussed further. It is however fundamental to an appreciation of the detrusor function during voiding, as is discussed below. The most convenient parameters that can be used to characterize detrusor dynamics are the detrusor pressure $p_{det}(t)$, and the urinary flowrate $Q(t)$. (Here, a measurement of the kinetic energy of the outlet stream is not essential since the urethral flowrate is always determined within the proximal urethra - see section 1.3.1.2[i]) . The detrusor is the primary energy source of micturition. During a voiding cycle, the detrusor converts stored biochemical energy into mechanical work by expelling a volume of urine against an outlet resistance within a finite time period. The

---

[i] The velocity of the exit stream is however dependent on the geometry of the external meatus. The exit kinetic energy thus becomes important in any evaluation of distal urethral strictures.

bladder has also been shown to store a limited quantity of energy for contracting, and "recharge" between successive contractions. Functionally, the bladder is thus a limited energy storage device. The quantity of energy stored (and thus the ability of the detrusor to do work, or generate power) has been shown to increase with bladder filling[5].

The conversion of biochemical energy to mechanical work in the detrusor is not ideal, and some mechanical and thermal losses are incurred. The mechanical work generated during a contraction can be divided into two components: the external work, and the internal work. The external work is defined as the work that can be measured in terms of a detrusor pressure and a volume voided (i.e. the flow work). The internal work is defined as the work done to elongate the elastic elements in series within the detrusor wall (Schäfer[5]), and is described only during the isometric portion of a detrusor contraction. (An isometric contraction refers to the period between the initiation of a contraction and the commencement of flow - i.e. when the detrusor pressure rises with zero flow). In a healthy bladder, the duration and strength of an isometric contraction vary in proportion to the outlet resistance. If losses are assumed negligible[4], the total bladder work can be defined as the sum of the internal work W_{int} and external work W_{ext}.

$$W_{total} = W_{ext} + W_{int} \tag{11}$$

As shown in equation (9), the external work is related to the kinetic energy of the urethral flow at any given point along the urethra. The external work can be easily calculated from the external voiding power $P_{ext}(t)$, defined as the product of the instantaneous (and corresponding) detrusor pressures $p_{det}(t)$ and flow rates $Q(t)$,

$$P_{ext}(t) = p_{det}(t)Q(t) \tag{12}$$

with the external voiding work defined as the time integral from time t = 0 to the terminus of voiding t = t_f of the external voiding power.

$$W_{ext} = \int_0^{t_f} P_{det}(t)Q(t)dt \qquad (13)$$

However, since no flow occurs during the isometric portion of a bladder contraction, this relation reduces to:

$$W_{ext} = \int_{t_v}^{t_f} P_{det}(t)Q(t)dt \qquad (14)$$

where, t_v is the time at which flow commences. This relation between the detrusor pressure, the flowrate, the external voiding power, and the external voiding work is schematically shown in Figure 1.8.

— isometric p_{det}
...... voiding p_{det}
— flow rate Q

$$P_{ext} = P_{det} \cdot Q$$

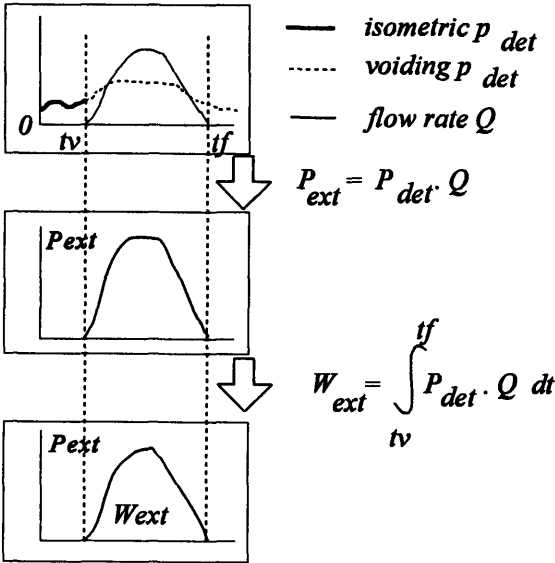$$W_{ext} = \int_{tv}^{tf} P_{det} \cdot Q \; dt$$

Figure 1.8 Schematic representation of relation between detrusor pressure P_{det}, flow rate Q, external voiding power P_{ext}, and external voiding work W_{ext}. Adapted from Schäfer, W. Detrusor as the Energy Source of Micturition. *Benign Prostatic Hyperplasia*. F. Hinman Jr (Ed). p 452.

Schäfer[5] has proposed that the internal voiding power $P_{int}(t)$ can be estimated from the pressure change dp/dt at a given volume $V(t)$ as:

$$P_{int}(t) \sim V(t)\, dp/dt \qquad (15)$$

The internal work $W_{int}(t)$ can thus be estimated as the time integral from $t = 0$ to the time of flow commencement $t = t_v$ of the internal voiding power:

$$W_{internal}(t) = \int_0^{t_v} V(t)\frac{dp}{dt}dt \qquad (16)$$

Since the bladder volume is constant during an isometric contraction, equation (10) can be reduced to:

$$W_{internal} = V_o \int_{p_o}^{p_v} dp = V_o(p_v - p_o) \qquad (17)$$

where, V_o is the filled bladder volume, p_v is the bladder pressure at the commencement of flow, and p_o is the bladder pressure at the initiation of the contraction[ii]. This formulation of the internal work merits a closer analysis. Recently, a continuous occlusion study[6] showed that during an isometric contraction, the detrusor pressure rises to a maximum, and then declines towards baseline. Such a contraction is schematically shown in Figure 1.9.

Here, the isometric contraction extends from time $t=0$ and a baseline detrusor pressure p_{det}^o to time $t=t_2$ and a pressure p_{det}^*, with the peak isometric pressure p_{det}^{max}

[ii] Since this work is computed from the product of a volume and a pressure difference (as opposed to the product of a pressure and a volume difference), strictly speaking, it represents a complementary work term.

occurring at time $t=t_{peak}$. If one attempts to compute the internal work done between $t=0$ and $t=t_2$ using equations (16) or (17), the internal work appears simply as the product $V_o(p_{det}{}^*-p_{det}{}^o)$.
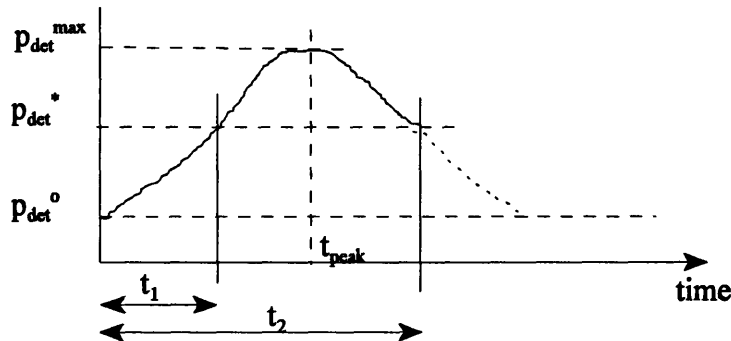

Figure 1.9 Schematic of the detrusor pressure behavior during an isometric contraction as characterized by the continuous occlusion study. The contraction begins at time $t=0$ and continues to time $t=t_2$. The time t_1 represents the time to first reach the detrusor pressure $p_{det}{}^*$.

By considering only the beginning and end pressure points $p_{det}{}^o$ and $p_{det}{}^*$, equations (16) and (17) effectively consider only the work required to *first* reach $p_{det}{}^*$ (i.e. the work done from time $t=0$ to time $t=t_1$) and ignore all work done between t_1 and t_2. It is possible to formulate the concept of internal work in this manner only if the detrusor work done to increase intravesical pressure between the times $t=t_1$ and $t=t_{peak}$ is stored as elastic energy that can be fully recovered between the times $t=t_{peak}$ and $t=t_2$. Equations (16) and (17) thus implicitly assume that a detrusor isometric contraction can be modeled as shown in Figure 1.10.

Here, an isometrically contracting detrusor is modeled as a voltage source V charging a variable capacitance C (the capacitance is used to model the bladder tissue that is assumed to store elastic energy). Since all stored energy is assumed to be fully recoverable, the connections between the voltage source and capacitance are modeled as having a zero resistance. An increasing detrusor contractile force can be modeled by

individually switching on voltage sources with successively higher voltages *V1*, *V2*... using the corresponding switches *S1*, *S2*... (The reader should note that the voltage *V* and electrical charge *q* in the electrical domain are equivalent to the pressure *p* and volume V_o in the fluidic domain respectively).
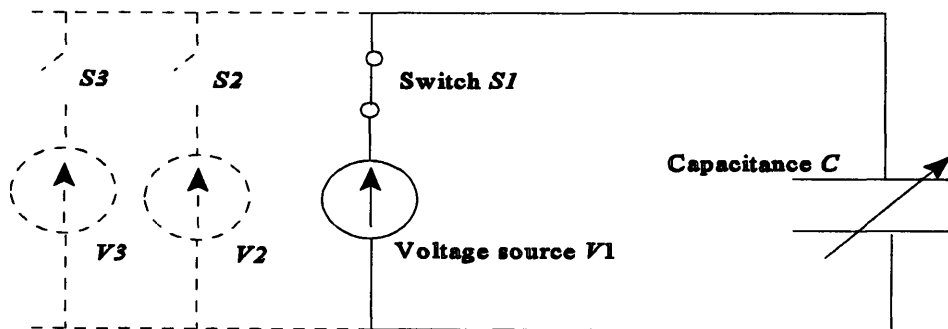

Figure 1.10   The isometrically contracting detrusor as modeled by equations (16) and (17).   The contracting detrusor is modeled as a voltage source *V* (attached across Switch *S1*) charging a variable capacitance *C* through a resistanceless wire.   An increasing detrusor contractile force can be modeled by individually switching on voltage sources with successively higher voltages *V1*, *V2*... using the corresponding switches *S1*, *S2* ...

The energy available to drive urethral flow at a given detrusor pressure (i.e. the elastic energy as referred to by equations (16) and (17)) is modeled by the electrical energy *E* stored in the capacitor *C* at a given voltage *V*. This stored energy is defined as $E = \frac{1}{2}(q^2/V)$. Given the identity *q=CV* relating the capacitance *C*, voltage *V*, and electrical charge *q*, this energy can be written as $E = \frac{1}{2}(qV)$.

That Figure 1.10 models equations (16) and (17) can be verified as follows: Since an isometric contraction is being considered, the bladder volume must remain constant for all detrusor pressures. The capacitor in Figure 1.10 used to model the bladder must therefore maintain a constant electric charge *q* for all applied voltages *V* (a variable capacitor is used in this model since the identity *q=CV* must be satisfied when the charge *q* is held constant for a varying voltage *V*). The change in the stored electrical energy Δ*E*

between two voltages V_1 and V_2 ($V_2 > V_1$) can now be computed as $\Delta E = 1/2q(V_2 - V_1) = 1/2q\ \Delta V$. Given the equivalency between the fluidic and electrical variables described previously, this relation translates into the fluidic domain as $\Delta E \propto V_o \Delta p$, which is the functional format of equations (16) and (17).

Although this formulation is very convenient, whether it adequately represents the contractile process within a detrusor smooth muscle cell must be examined. The smooth muscle contractile process is summarized below. If a more detailed description is required, the reader is directed to a medical physiology text such as Guyton, A.C., *Textbook of Medical Physiology*.

Smooth muscle cells use actin and myosin filaments for their contractile function. In smooth muscle, actin and myosin filaments are not arrayed as serial sarcomeres as in skeletal and cardiac myocytes. Rather, the actin filaments are attached to dense bodies with the myosin filaments interspersed between the actin filaments (the dense bodies are equivalent to the Z disks of the skeletal myocytes). The membrane depolarization of a smooth muscle cell is dependent on the activation of slow L-type calcium channels (as opposed to the fast sodium channels in skeletal muscle). Since these channels typically generate depolarizations with a slow upstroke, and since the impulse propagation velocity is proportional to the rate of change of the upstroke, the velocity of impulse propagation in smooth muscle is relatively slow.

Smooth muscle cells typically use calcium as the major second messenger in the excitation-contraction coupling process. Here, cytoplasmic calcium (accumulated by the calcium influx through the L-type channels) activates the calcium dependent regulatory protein calmodulin. Calmodulin in turn activates the enzyme myosin kinase which phosphorylates the regulatory chain on myosin heads allowing the myosin heads to form cross bridges with adjacent actin filaments (skeletal muscle uses the Troponin-Tropomyocin regulatory complex for this process). During this cross bridge formation, myosin heads typically have bound ADP. Once cross bridges have formed, the myosin heads bend, moving the myosin filament relative to the actin filaments, and thus potentiate a myocyte contraction. Once bent, the myosin heads release ADP and bind ATP. ATP

bound myosin heads have a reduced affinity for their actin binding sites resulting in a gradual dissociation of the cross bridges. The free myosin heads will then hydrolyze ATP to ADP and use the resultant energy to straighten themselves (from their previously post-contractile bent configuration). Since the straightened myosin heads will again have bound ADP (residual from the preceding ATP hydrolysis) the contractile cycle can now repeat. The cycling frequency of cross bridges in smooth muscle is slower than in skeletal muscle. Since this cycling rate effectively defines the rate of ATP consumption, smooth muscle cells are able to contract for relatively longer periods (with respect to skeletal myocytes) on a given ATP store.

At contraction termination, the L-type calcium channels close while energy dependent calcium ATPase pumps remove calcium from the smooth muscle cytoplasm and thus deactivate calmodulin. The regulatory enzyme myosin phosphatase will also become active and dephosphorylates the regulatory light chain inhibiting the formation of cross bridges. The sequence of contractile events will thus terminate, and the cell will return to its resting state.

The ability of a smooth muscle cell to maintain a contraction, is, therefore, dependent upon the presence and interaction of numerous biochemical factors. Of these, the single factor most susceptible to depletion is ATP. Given the preceding information, one can expect that if the rate of ATP consumption during a contraction exceeds the rate of its generation, a myocyte will be unable to contract, and fatigue. Since ATP is required for the release of cross bridges, one would also predict that with ATP depletion myocyte relaxation will be impaired resulting in a rigor like low compliance (i.e. inelastic) condition. The electrical model described in Figure 1.10 is simply unable to account for this complex behavior. Specifically, by assuming that all energy expended in increasing detrusor pressure can be recovered, the model implicitly assumes that the isometrically contracting detrusor muscle cells will always be perfectly elastic. This is equivalent to assuming that the myocytes will not fatigue. This assumption is not physiologically valid, since all myocytes fatigue after a period of continued contraction. In fact, the decline in the detrusor pressure from a peak value as described in the continuous occlusion study

(and schematically shown in Figure 1.9) represents such a gradually fatiguing detrusor.

The concept of a fully recoverable internal work thus cannot represent an isometric contraction progressing beyond a peak detrusor pressure and into fatigue conditions. With the onset of fatigue, the energy available to drive flow through the urethra at a given detrusor pressure and the work done in increasing the detrusor pressure to that level are not equal. It is therefore inappropriate to describe an isometric contraction in terms of an internal work. Rather, an isometric contraction should be described using a more generalized energy available to drive flow through the urethra. The reader should note that in reality, it is this energy, and not the internal work that is accounted for by the shear work term in the first law of thermodynamics.

A modified version of the model depicted in Figure 1.10 incorporating the effects of fatigue is suggested below. Here, an internal resistance R has been inserted in series with the capacitance C, while the voltage source has been replaced with a battery B. The internal resistance is used to model the effects of fatigue, while the battery is used to model a detrusor smooth muscle cell with a limited stock of ATP.
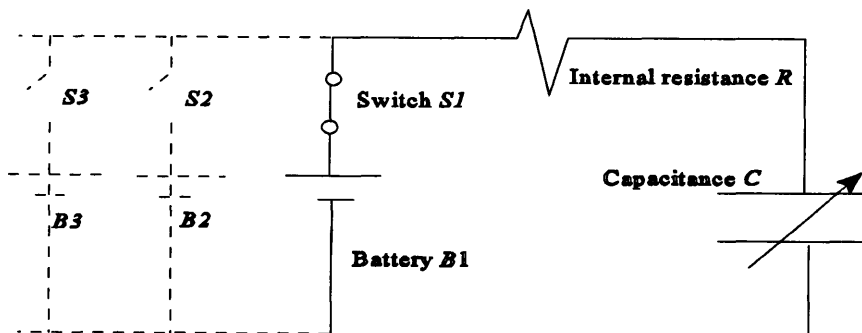

Figure 1.11   Modified model for assessing the energy available to drive urethral flow at a given detrusor pressure. The internal resistance R is used to model the effects of fatigue, while the batteries *B1, B2...* are used to model the detrusor smooth muscle cells with a limited ATP energy store.

The formulation of the energy available to drive urethral flow or "internal work" as formulated by equations (16) and (17) is thus neither ideal nor absolute. Ideally, it would be possible to explicitly account for this energy in terms of the moles of ATP hydrolyzed or oxygen consumed during the entire isometric contraction. At present however, such a formulation is not available. Schäfer's approach will thus be used in the subsequent analyses as a first approximation. The term "internal work" will also be retained in describing an isometric contraction. The reader should however keep in mind the limitations of equations (16) and (17), and this terminology when reviewing the relevant results in section 3.1.2.

Within the limits of a maximum isometric pressure (at zero flow) and a maximum flow rate at zero pressure, the relation between p_{det} and Q for a given bladder power level is inverse. Lower Q and higher p_{det} are characteristic of outlet obstruction. This phenomenon was initially postulated as an active compensatory action by the bladder (in response to the increased outlet resistance). It has also been argued[5] to result purely from the passive inverse relation between p_{det} and Q (refer figure 1.5). The definite mechanism has however not yet been fully elucidated.

Because of the depressed flowrates, an obstructed bladder must perform more work to expel a given volume of urine than would an unobstructed bladder. However, the bladder is a limited energy storage device. Therefore, for a given bladder volume, micturition from an obstructed bladder can be expected to terminate before the bladder is completely emptied. Post void residual urine is thus also characteristic of an obstructed bladder.

1.3.1.2   Distensible tube approach

Here, the urethral impedance is interpreted from a plot of the detrusor pressure vs. urine flowrate. The graph showing the relation between the instantaneous and corresponding detrusor pressures and flowrates during voiding is termed a pressure-flow
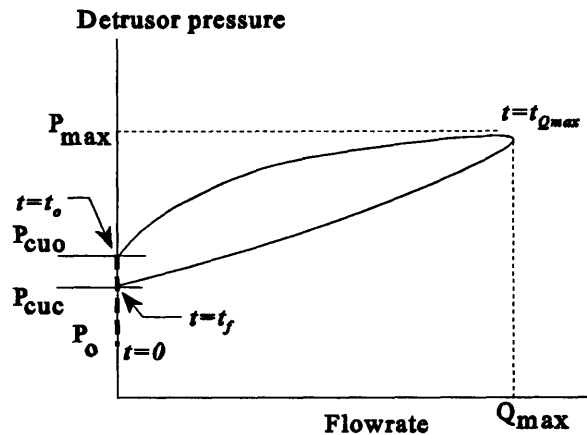
(PQ) curve. An idealized PQ curve is shown below:

Figure 1.12 An idealized pressure-flow (PQ) curve

Urethral flow will commence only after the detrusor pressure has exceeded a critical urethral opening pressure p_{cuo}. Similarly, at the terminus of voiding, flow will cease once the detrusor pressure has fallen below a critical urethral closure pressure p_{cuc}. If the urethra behaves as a perfectly elastic tube, and if no muscular relaxation and/or passive viscoelastic relaxation of the bladder outlet is present, the p_{cuc} will equal the p_{cuo}.

The urethral resistance relation (URR) represents the initial effort to use the distensible tube model to describe outlet resistance. However, since the URR considered pressure-flow relations through the entire voiding cycle, its interpretation was complex, and hence did not present a convenient diagnostic tool. An alternate method for outlet resistance computation is the passive urethral resistance relation (PURR). By basing its resistance computation upon the pressure-flow relation from peak flow to voiding terminus, the PURR is simple and convenient to both construct and interpret, and has become the modality of choice for the clinical evaluation of outlet resistance. The PURR, its derivation and applications, are discussed further in section 1.5.

A fundamental characteristic of collapsible (distensible) tube flow is the existence of a choke point termed a flow controlling zone. The flow controlling zone of the urethra normally lies within the membranous urethra. Within this zone, the urine flowrate is maximized via a process termed flow limitation. Once flow limitation has occurred, the flowrate becomes essentially effort independent. That is, until flow limitation is reached, straining (i.e. increased voiding effort) will produce increased flowrates. However, once flow limitation is reached, added effort will not produce any increase in flow. This phenomenon can be quantified as follows:

The transmural pressure p_{tm} along the urethra is defined as the difference between the pressure inside the urethra p_i and outside the urethra p_o. For the membranous urethra, this outside pressure is, to a first approximation, the abdominal pressure p_{abd}. Thus, the transmural pressure at any point along the membranous urethra is:

$$p_{tm} = p_i - p_{abd} \qquad (18)$$

The Bernoulli equation can be used to relate the detrusor pressure p_{det} to the p_i in terms of a proximal fluid velocity v_{prox} and density ρ as shown below. (It should be noted that since flow within the bladder itself is approximately zero, p_{det} is effectively a stagnation pressure).

$$p_{det} = p_i + \frac{1}{2} \rho v_{prox}^2 \qquad (19)$$

This expression assumes steady flow through a tube of constant cross sectional area, with no viscous or other losses present. (Viscous effects can be accounted for by adding a frictional pressure drop Δp_{fr} to the right-hand-side of equation (19), but will not be considered here since flow limitation occurs even if frictional losses are not explicitly considered, as will be shown below).

Equation (19) can be re-written in terms of the urinary flowrate Q by substituting $Q = v_{prox}A$, with A, the local cross sectional area. Thus,

$$p_{det} = p_i + \frac{1}{2}\rho\frac{Q^2}{A^2} \qquad (20)$$

and,

$$Q = A\sqrt{\frac{2}{\rho}(p_{det} - p_i)} \qquad (21)$$

Equation (21) can also be re-written as:

$$Q = v_{prox}A = A\sqrt{\frac{2}{\rho}[(p_{det} - p_{abd}) - (p_i - p_{abd})]} = A\sqrt{\frac{2}{\rho}(H - p_{tm})} \qquad (22)$$

with H defining the total pressure head relative to the abdominal pressure. Thus, the problem of flow limitation can be reduced to an estimation of the largest possible attainable flowrate for a given total pressure head relative to abdominal pressure, as effort is increased. (In this context, H can be considered a local driving pressure). Hence, flow limitation will occur when:

$$\frac{dQ}{dp_{tm}}\Big|_{H=const} = 0 \qquad (23)$$

With $Q = v_{prox}A$, this condition can be evaluated as follows:

$$\frac{dQ}{dp_{tm}} = 0 \rightarrow A\frac{dv_{prox}}{dp_{tm}} + v_{prox}\frac{dA}{dp_{tm}} = 0 \qquad (24)$$

Now, by using equation (22),

$$\frac{dv_{prox}}{p_{tm}} = \frac{1}{2}[\frac{2}{\rho}(H-p_{tm})](\frac{2}{\rho})(-1) = -\frac{1}{pv_{prox}}$$ (25)

The evaluation of the dA/dp_{tm} term requires the introduction of a new variable, the speed of pressure wave transmission along the urethral wall c, which is a function of fluid inertia (i.e. density ρ) and local urethral specific compliance $(1/A)dA/dp_{tm}$. The specific functional expression of c is as follows:

$$c = \sqrt{\frac{1}{\rho}[\frac{1}{A}\frac{dA}{dp_{tm}}]^{-1}}$$ (26)

and,

$$\frac{dA}{dp_{tm}} = \frac{A}{\rho c^2}$$ (27)

Thus, equation (24) reduces to:

$$\frac{dQ}{dp_{tm}} = 0 \rightarrow -A\frac{1}{pv_{prox}} + v_{prox}\frac{A}{\rho c^2} = \frac{A}{\rho}(\frac{v_{prox}^2}{c^2}-1) = 0$$ (28)

From equation (28), it is evident that the maximum flowrate Q_{max} will occur when,

$$v_{prox} = c$$ (29)

Thus, the flowrate will be maximized (i.e. flow limitation will occur) once the flow velocity in the membranous urethra v_{prox} is equal to the wave speed c. The functional expression of the maximum flowrate Q_{max} therefore becomes:

$$Q_{max} = cA = \sqrt{\frac{A^3}{\rho}(\frac{dA}{dp_{tm}})^{-1}}$$ (30)

Functionally, the flow controlling zone will govern the impedance presented to the bladder, and isolate the bladder from the influences of more distal regions of the urethra.
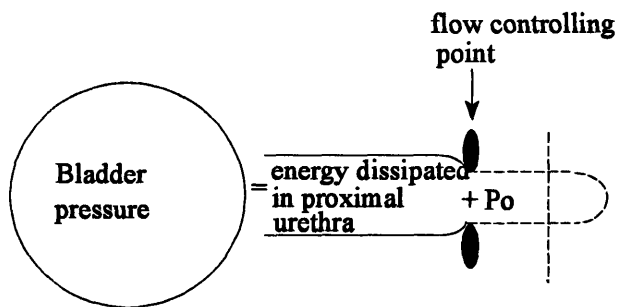

flow controlling
point

Bladder
pressure

= energy dissipated
in proximal
urethra

+ Po

Figure 1.13 Energy balance during voiding according to the distensible tube approach. When a flow controlling zone is present, p_o is the total pressure needed locally to overcome the elasticity of the flow controlling zone. p_o depends upon the relevant flow rate, and the mechanical properties of the controlling zone. The distal parts of the urethra, and the external stream (dotted) have no effect on either the proximal urethra or p_o, and thus do not contribute to urethral impedance.

The distensible tube approach classifies a urethra as obstructed if its impedance is above a value considered normal. Under obstructive conditions, urethral impedance will be dominated by the obstruction (i.e. the region of obstruction will contain the new flow controlling zone, with its local area and compliance defining Q_{max}).

Urodynamic techniques such as a Micturitional Urethral Pressure Profile (MUPP) can be used both to detect the location of an obstruction and to estimate its severity - the obstruction will be located at the site of the static (or total) pressure drop, while the severity of obstruction will be proportional to the magnitude of the pressure drop.

CZ$_O$ - compressive zone: obstructed
CZ$_N$ - compressive zone: normal

Pressure

bladder outlet obstruction

normal

bladder   CZ$_O$ CZ$_N$ meatus

distance
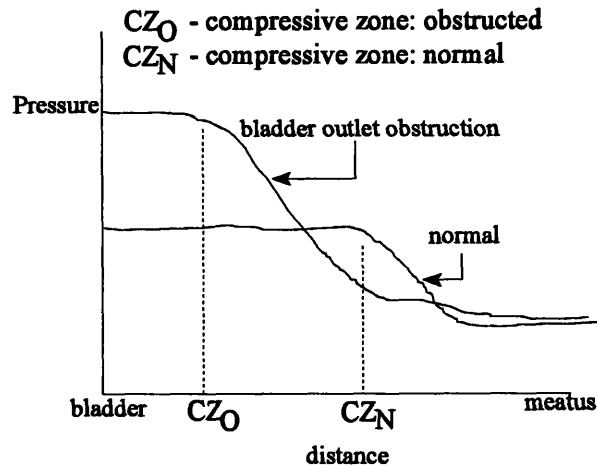
Figure 1.14 Expected micturitional urethral pressure profiles for a normal and proximally obstructed male.

1.4   Benign Prostatic Hyperplasia (BPH)

1.4.1   Pathology of Benign Prostatic Hyperplasia

The prostate is a compact organ related to the male genito-urinary tract. Anatomically, it is positioned at the bladder neck, and surrounds the prostatic urethra (refer Figure 1.3). BPH refers to the non-cancerous growth of prostatic mass. Strictly speaking, such growth may occur from either the hypertrophy, or hyperplasia of stromal and glandular cells. However, in general, the terms hyperplasia and hypertrophy are used interchangeably in describing BPH. The glandular and stromal hyperplasia associated with BPH, while substantially increasing prostatic tissue volume, will also alter the

geometry and architecture of the prostate gland. The elastic properties of the prostatic capsule will determine whether BPH will compress the prostatic urethra. Prostates with predominantly fibromuscular components may cause outlet obstruction by altering urethral compliance, and impeding urethral flow[7].

Enlarged lateral prostate lobes will compress the urethral lumen into an elongated, broad, ribbon like channel. Growth of the median lobe may, however, be confined by the urethral musculature. If so, a growing median lobe will expand in a sub trigonal direction, elevating or angulating the internal urethral meatus forward. If not, the median lobe may push into the bladder lumen, and ultimately result in a "ball-valve" obstruction of the internal meatus. BPH associated urethral obstruction itself will result from the elongation, tortuosity and compression of the posterior urethra.

1.4.2   Incidence

The prostate does not maintain a uniform growth rate throughout the life time of an individual. Prostatic mass increases slowly from birth to puberty, accelerates between puberty and the thirtieth year, and then remains constant for about a decade.

Hyperplasia/hypertrophy of the prostate could begin around the age of 40 years. If so, prostate mass will begin a rapid growth until an individual's death. (Alternately, the prostate may even begin to atrophy, and progressively decrease in size). BPH is characteristically a disease of men aged over 40 years. By the age of 75 years, the probability of prostatism increases to 75%[8].
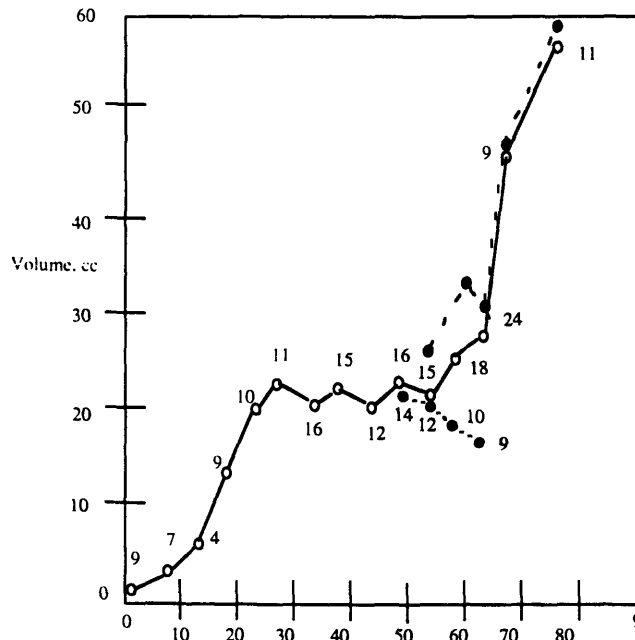
Figure 1.15 Mean volume of the prostate by age group. Hollow circles represent the mean volume of all prostates in all age groups, shaded circles represent the mean volumes of the normal prostates, and black circles represent those of hyperplastic prostates. (From Swyer, G.I.M, Anat., 1944)
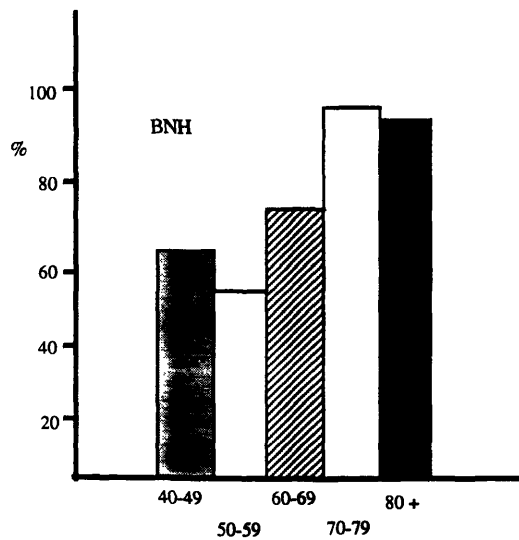
Figure 1.16 Incidence ratio of benign nodular hyperplasia (BNH) with the age in 206 consecutive autopsies. (From Harbitz, T.B., and Hangen, O.A.,: Acta Pathol. Microbiol. Scand. [A], 80:766, 1972).

1.4.3   Diagnosis

The most commonly used tools for BPH diagnosis include physical examinations, patient symptom questionnaires (AUASI, I-PSS), and urodynamic assessments such as cystometry, uroflometry and voiding profilometry (MUPP).   For example, the site (and degree) of an obstruction can be estimated using a Micturitional Urethral Pressure Profile (MUPP); and urethral impedance can be estimated using pressure-flow relations.   Despite these techniques and a host of related technologies, some confusion regarding the accurate diagnosis of obstructive BPH vs. irritative prostatism still persists.   This can be attributed to a number of reasons.   For example, a patient may be under medications that directly or indirectly influence the function of the bladder and its outlet.   Alternately, a patient may suffer from hidden subclinical neurogenic conditions such as diabetic autonomic neuropathy, or cerebrovascular disease that overtly mimic BPH.   Moreover, the effects of aging on the mechanics of the bladder at present are not well understood.   The diagnostic value of the prostatism complex in detecting obstructive BPH is also marginal since its symptoms do not necessarily indicate prostate enlargement or outlet obstruction.   Even those symptoms considered unequivocal evidence of outlet obstruction such as acute urinary retention and post void residual volume, may be a result of detrusor dysfunction as opposed to BPH.   At present, the most efficient methods of BPH diagnosis are urodynamic assessments such as the MUPP.

1.4.4   Treatment

The symptoms of adult male voiding dysfunction (prostatism), either obstructive or irritative in nature, are highly non-specific, and do not necessarily indicate the underlying pathophysiology of the voiding dysfunction.   Nonetheless, at present, prostatism is mostly

associated with BPH induced outlet obstruction. Hence, the most common treatment for prostatism is the Trans Urethral Resection of the Prostate (TURP), a procedure where sections of the enlarged prostate are surgically removed. In the United States alone, approximately 500,000 TURPs are performed annually at a cost of about $5 billion. In a health interview study on 471 patients, prostatic surgery was found to be effective in 93% of severely symptomatic patients, but effective in only 79% of the moderately symptomatic patients[9]. A long term follow-up (5-8 years) study of patients with prostatism revealed that 24% of those who had elective prostatectomies regained their symptoms[10]. Both studies indicate that a significant portion of TURPs performed fail to alleviate the symptoms of prostatism. Surgical intervention must thus be more judiciously applied than at present. This becomes extremely critical in the present era of spiraling health care costs and dwindling funding. Alternate conservative treatment methods such as watchful waiting or pharmacological management must also be designed and attempted. But for all this, a more comprehensive understanding of the pathophysiology of prostatism than presently available is required.

1.5   Current status of research

Morphological changes such as a denervation of the bladder wall, and an infiltration of connective tissue between detrusor muscle bundles, and physiological changes such as detrusor instability and urinary retention have been observed in human males with outlet obstruction. Suitable animal models have been used to investigate the sequence and inter-relations of these pathologies[11,12]. Much work has also been performed to assess micturition and urethral impedance from a fluid dynamics stand point.

Several urodynamic parameters have been used to characterize detrusor function. Of these the detrusor pressure p_{det} and the urinary flowrate Q can be measured the most

accurately, and are the most accessible. Voiding dynamics are thus best characterized using p_{det} (or p_{ves}) and Q data as in the pressure-flow (PQ) curve introduced in section 1.3.1.2.

Many attempts have been made to describe, and explain the relationship between p_{det} and Q. All have attempted to do so by defining some form of urethral resistance. The early attempts treated micturition as a simple hydrodynamic process, and concentrated on reducing the complex voiding dynamics to a single number using urethral resistance factors. The general form of a resistance factor is:

$$R_1 = \frac{p_{det}^{n}}{Q^{m}} \qquad\qquad n = 0.5 \text{ or } 1; \ m = 1 \text{ or } 2. \qquad\qquad (31)$$

These factors are, however, unsuitable to describe urethral resistance for a variety of reasons. For example, resistance factors are based on rigid pipe theories that do not extend to distensible tubes. They also treat only the point of peak flow, and thus minimize the information that can be extracted from a PQ curve. Physiologically, the practice of reducing voiding dynamics to a single number can also be highly misleading. The URR corrected some of these deficiencies, but was wanting in its complexity (refer section 1.3.1.2).

At present, bladder outlet resistance is defined, quantitatively and qualitatively, using a passive urethral resistance relation PURR. Here, outlet resistance is estimated from the (time independent) slope of a PQ curve from peak flow to voiding terminus (i.e. zero flow). This period will be termed the passive duration of voiding (a discussion of the implications of this terminology will be postponed until section 3). By limiting itself to this region, a PURR eliminates much of the complex, time dependent pressure-flow relations associated with active changes in the bladder outlet. Further, by constructing the PURR from the path of least (relative) resistance, it can be assumed that the PURR will be very closely related to the effective morphology of a perfectly relaxed bladder outlet.
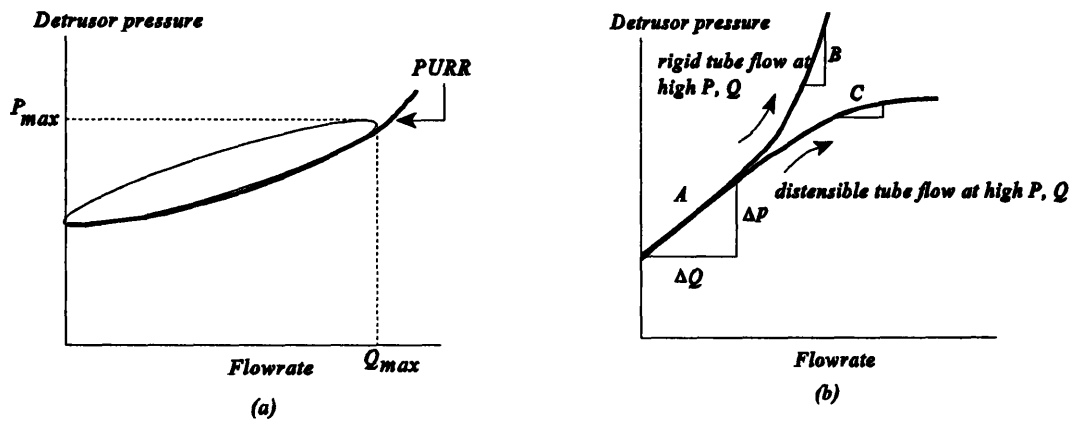
Figure 1.17 (a) Idealized PURR for a voiding cycle. (b) The trend in the local slope of a PQ curve provides information regarding the behavior of the urethra at high pressures and flow rates. If the slope increases as from A to B, rigid tube flow (constant cross sectional area) is implied. If the slope decreases as from A to C, distensible tube flow is implied. (Adapted from Schafer, W. The Contribution of the Bladder Outlet to the Relation Between Pressure and Flow Rate During Micturition. *Benign Prostatic Hyperplasia*. F. Hinman Jr. (Ed). p 474).

The slope of the PQ curve (dP/dQ) can either be positive or negative. A positive slope occurs during a period of either a constant urethral resistance or a slow passive change. A steeper slope indicates a higher relative resistance. If the slope increases with increasing pressure and flow rates, rigid tube flow (i.e. a constant cross sectional area) at these pressures and flowrates is implied. Conversely, if the slope decreases, the urethra will be as distensible at high pressures and flow rates as it is at low pressures and flow rates. Since a negative slope most often implies an active contraction of the bladder outlet musculature, only positive slopes are incorporated into the PURR.

As mentioned previously, flow will commence only once detrusor pressure has risen above a critical urethral opening pressure p_{cuo}. The effective driving pressure of the urine flow can thus be described as the difference between the detrusor pressure p_{det} and the p_{cuo}.

$$P_{dp} = P_{det} - P_{cuo} \qquad\qquad (31)$$

At this juncture, two issues must be addressed. First, present literature refers to the pressure at which the PURR intersects the pressure axis as the minimum urethral opening pressure p_{muo}. Physiologically however, this pressure is a *closure* pressure (i.e. the critical closure pressure p_{cuc} defined in section 1.3.1.2). Thus, to define the p_{muo} equal to the p_{cuo} is to constrain the critical urethral opening and closure pressures to be equal (or alternately, define the urethra as a perfectly elastic tube - refer section 1.3.1.2). Since this criterion is not necessarily valid, the p_{muo} (i.e. the p_{cuc}) and the p_{cuo} will be considered distinct entities in the subsequent discussions. Second, although not explicitly shown, the static fluid pressure in the proximal urethra contains an abdominal pressure component p_{abd} (refer equation (18)).

The Bernoulli equation (assuming steady, non-viscous flow) can be used to express the proximal flow velocity v_{prox} in terms of the p_{dp}, and the fluid density ρ:

$$P_{dp} = P_{det} - P_{muo} = (\frac{\rho}{2})v_{prox}^2 \qquad (32)$$

The continuity equation can be used to relate the flow rate Q, the proximal velocity at the compressive zone v_{fcz}, and the effective cross sectional area of the flow controlling zone (A_{fcz}):

$$Q = v_{fcz} A_{fcz} \qquad (33)$$

The external voiding power as expressed by equation (12) is:

$$P_{ext} = p_{det} \cdot Q \qquad (12)$$

It should be noted that equations (33) and (12) together, relate the force of contraction in terms of p_{det} to the contraction velocity in terms of flow velocity v_{prox} and thus define the muscle mechanics requirement of micturition.

When defining urethral resistance, the PURR makes the additional assumption that

the bladder pressure is linearly proportional to the (flow rate)^2, and is of the form:

$$p_{det} = p_{muo} + RQ^2 \qquad (34)$$

where R is a constant representing the slope of the PURR, and can be obtained analytically. This constant R represents the outlet resistance as computed by the PURR. Combining equations (32), (33) and (34):

$$\frac{\rho}{2}v_{fcz}^2 = RQ^2 = R(v_{fcz}A_{fcz})^2 \qquad (35)$$

The cross sectional area of the flow controlling zone A_{fcz} can now be expressed as:

$$A_{fcz} = \sqrt{\frac{\rho}{2R}} \qquad (36)$$

The cross sectional area of the flow controlling zone itself, as described by equation (36), is defined by the time independent parameters ρ and R. Thus, the PURR model describes a (opened) flow controlling zone as a rigid tube with a cross sectional area A_{fcz}. By assuming a constant A_{fcz}, the PURR further asserts that the static pressure within the flow controlling zone will remain constant at p_{cuo}. The PURR is thus a graphical representation of the pressure-flow characteristic of a fully opened flow controlling zone, that effectively dominates the passive urethral resistance of the entire urethra with its R and p_{cuo} values (i.e. the compressive zone exhibits the highest p_{cuo} and R values of all urethral segments, and thus governs the PURR).

A normal PURR is described by a low p_{cuo} and a low R value. These parameters together define the relatively low bladder energy per unit volume voided (i.e. relatively high flow rates for relatively low bladder pressures) characteristic of normal voiding. Since the PURR is intimately associated with a passive outlet morphology, any change in

this morphology (i.e. outlet obstruction) can be expected to manifest in an altered PURR. Two types of obstructions can be defined according to their influence on the PURR.

i   **Compressive obstruction:**   This type of obstruction results in an elevated p_{muo} and p_{cuo} with a constant R. Physically, such an obstruction implies that the compressive zone now requires a higher detrusor pressure to open, but will open to an unchanged effective cross sectional area. The higher p_{cuo} implies that the driving pressure for a given detrusor contraction will be reduced (refer equation (31)).

ii   **Constrictive obstruction:**   This type of obstruction results in an unchanged p_{cuo} with a higher R. Physically, this implies that the opening pressure for the compressive zone will remain unchanged, while its (opened) effective cross sectional area will decrease. Since the p_{cuo} is unchanged, the effective driving pressure will also remain unchanged.

Compressive obstruction   Constrictive obstruction
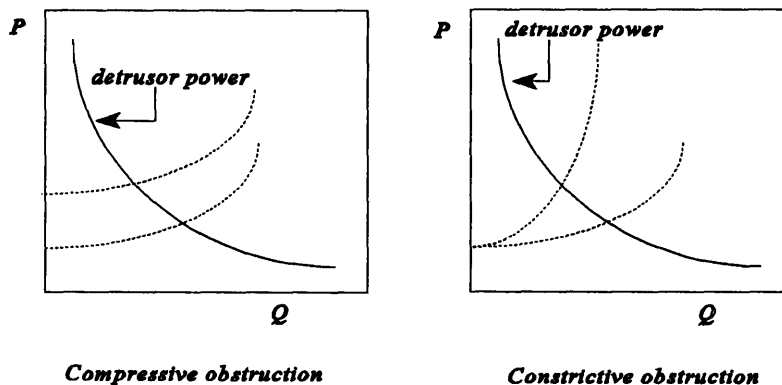
Figure 1.18 Changes in the PURR from compressive and constrictive obstruction. Note that the increase in pressure and decrease in flowrate with obstruction can be explained assuming unchanged detrusor function coupled to an altered outlet morphology, i.e. a changed PURR.

As shown in Figure 1.18, both obstruction types produce elevated peak detrusor pressures and depressed peak flow rates. However, only the constrictive obstruction will alter the relation between the two.

Compressive and constrictive obstructions also show markedly different voiding efficiencies. To prevent a post void residual volume, a detrusor must maintain power until the bladder is completely emptied. Therefore, the minimum muscle power at which bladder outflow can be maintained (P_{min}) becomes the critical parameter for residual-free voiding, and is a convenient parameter to define voiding efficiency. P_{min} itself can be defined in terms of a minimum voiding pressure p_{min} and an incremental flow rate. If this p_{min} is approximated to the p_{cuo}, then P_{min} can be expressed as (again, assuming $p_{cuo} = p_{cuc}$):

$$P_{min} = p_{cuo} \cdot \Delta Q \qquad (36)$$

Therefore, for a given bladder volume, and peak flow and pressure conditions, the compressive obstruction will show a higher P_{min}, and thus, lower voiding efficiencies. Consequently, post void residual volumes are more typical of compressive obstructions, than constrictive obstructions. In general, BPH is a compressive obstruction (although it may also possesses a constrictive component), while distal strictures are typically constrictive.

Dynamic changes in the bladder outlet (and thus dynamic changes in the urethral resistance) due to muscular contractions are treated separately using the dynamic urethral resistance relation DURR[13]. These changes are approximated using a relative difference ΔR defined as the difference between the potential flow rate as calculated using the PURR (Q^*) and the actual flow rate (Q), as a fraction of Q. The DURR is constructed by plotting ΔR over time.

$$\Delta R = \frac{Q^* - Q}{Q} \qquad (37)$$

1.6   Significance

The PURR method has been very successful in characterizing bladder outlet function. However, several issues require clarification. Primarily, it must be established how much insight into the entire micturitional process a PURR alone can provide. Because of its ease in construction and interpretation, it is very convenient to assess micturition using only a PURR. Such an effort may be fundamentally flawed in that a PURR itself is constructed using only a fraction of the entire voiding cycle (i.e using only the passive duration as discussed in section 1.5). This period may encompass as little as 33% of the total voiding time. Thus, strictly speaking, the PURR represents outlet characterization during only a significantly small window of the voiding process. Any effort to characterize the entire micturitional process using the PURR alone therefore implicitly assumes that no new and/or useful information is contained within the "non-passive" remainder of the PQ curve[i]. This hypothesis definitely merits investigation. In fact, there is no reason to assume any dependence between the information contained within the passive, lowest resistance region and the other (omitted) portion of a PQ curve. By ignoring much of the PQ curve, we may well be missing vital information on voiding dynamics. This issue will be a primary focus of the proposed study.

---

[i]   ideally, the lower portion of a PQ curve would represent the passive, lowest resistance region (i.e. the PURR), and the upper portion would represent the "non passive remainder" of the PQ curve.

Hypotheses:

(1)   The region of the pressure-flow curve representing pre-peak flow conditions is independent of the region representing post-peak flow conditions (characterized by a PURR).

(2)   The pre-peak flow region, essentially ignored by a PURR, contains information regarding voiding dynamics that cannot be obtained by manipulation of the PURR results.

(3)   During urodynamic analyses, flow in the urethra can be treated as laminar, and fully developed[viii].

Objectives:

This thesis will attempt to,

(1)   Characterize urethral flow and construct the urethral resistance relation using fluid dynamic parameters under obstructive and non-obstructive conditions.

(2)   Evaluate the detrusor power and energy relations during isometric and voiding contractions under obstructive and non-obstructive conditions.

(3)   Generate Reynolds numbers and entry lengths[ii] for urethral flows, and examine the validity of the fully developed laminar flow hypothesis.

(4)   Define a urethral pressure-area relation (a tube law), and evaluate changes in this relation under obstructive and non-obstructive conditions.

[ii]   These concepts are explained in section 3.2

2   Materials and Methods

Seven adult female, and two adult male dogs were used in this study. The effects of varying degrees of outlet obstruction on the voiding behavior of each animal were individually evaluated using pressure-flow (PQ) curves. All outlet obstructions were created using an inflatable sphincter cuff placed around the bladder neck.

Dog 1	Dog 2	Dog 3	Dog 4	Dog 5	Dog 6	Dog 7	Dog 8	Dog 9
F	F	M	M	F	F	F	F	F
Young	Young	Young	Old	Young	Young	Young	Young	Young

Table 2.1 Categorization of studies by sex of animal used. Females are denoted by "F" and males by "M".

2.1   Surgical procedure

All animals were premedicated with biotal (8mg/kg) and intubated with an endotracheal tube. A surgical plane of anesthesia was maintained with halothane 1-2%, and the animals were sustained with I.V. fluids (lactated Ringer's solution) throughout the surgical (and subsequent experimental) procedures. The animals' heart rates and blood pressures were continuously monitored, while their respiration was supported using a ventilator.

A lower abdominal midline incision was made through all layers of tissue exposing the urinary bladder, and the proximal urethra. Each ureter was isolated, and partially transected. Both ureters were catheterized anterograde using 3F pig tailed catheters from their transection points into the bladder. During the functional analyses, one catheter was used for filling, while the other was used for intravesical pressure measurements. Urine from the kidneys was drained by inserting a 1mm diameter polyethylene tube retrograde through each ureter (again from their transection points) into the corresponding kidney's renal pelvis (refer figure 2.1). All catheters and tubes were firmly attached to the ureters using silk ties.

A pubectomy was performed to expose the distal urethra running posterior to the symphysis pubis. In females, the entire urethral length was used for the experimental procedure. In males, the urethra was transected at the penile bulb sparing only the urethral length from the bladder neck to the symphysis pubis (i.e. leaving only the prostatic and membranous segments - approximately equal to the complete female urethral length).

Once the distal urethral orifice (external meatus in the female, and the point of transection in the male) was located, a tapered, stainless steel cannula (smallest diameter 3.5mm) was inserted, tapered end first, and stitched in place. The free end of this cannula was connected to a constant pressure head using a rigid polyurethane tube. This pressure head was maintained at bladder level to provide a constant back pressure to urethral flow.

A small transmural incision was made (at a measured distance from the bladder neck) on the distal urethra wall for a distal urethral pressure measurement. For this, a needle with a flanged tip was inserted into the incision until its flange completely penetrated the urethral wall. The needle was then manipulated until its flange was flush with the urethral epithelium, and stitched onto the outer urethral wall. The needle was flushed with 0.5% saline to ensure the stitches maintained a water-tight seal. The integrity of the urethral lumen was reconfirmed by filling the bladder with 0.5% saline and expelling the filled volume through the urethra by gently pressing the bladder wall, while checking for leaks.

Branches of the pelvic nerves innervating the bladder were next exposed bilaterally, and electrodes attached to them (all detrusor contractions under experimental conditions were created via electrical stimulation, as will be described shortly). During experiments requiring outlet obstruction, an evacuated sphincter cuff was placed and secured around the bladder neck (refer figure 2.1).
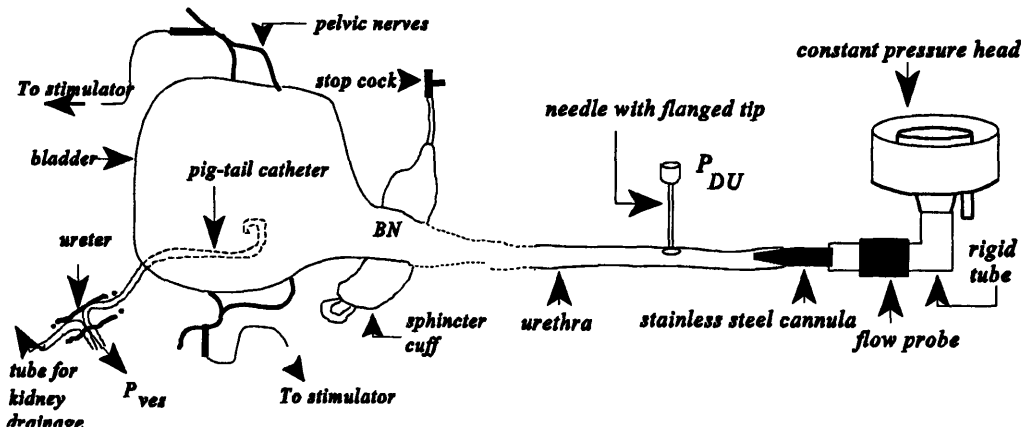
Figure 2.1 Schematic of experimental setup. Both ureters were arranged as the single ureter shown in the diagram. Of the two pig-tail catheters inserted into the bladder, one was used for pressure measurement, and the other for bladder filling. The catheter used for intravesical pressure measurement p_{ves}, and the needle with a flanged tip (to be used for distal urethral pressure measurement p_{DU}) were connected to separate (calibrated) pressure transducers. The catheter used for bladder filling was connected to an infusion pump. The (calibrated) flow probe was connected to an ultrasonic flowmeter. A third pressure transducer (not shown in diagram) was connected to the femoral artery to monitor blood pressure.

2.2   Functional evaluation

Two pressure transducers were calibrated between 0 - 50 cm H_2O using a water manometer. One was connected to the pig-tail catheter used for intravesical pressure measurement, and the other, to the needle used for distal pressure measurement. Both transducers were secured around bladder level such that the baseline pressures measured would approximate the resting bladder and distal urethral pressures. A Transonic Systems ultrasonic flow probe was calibrated between 0 - 500 ml/min, and clamped onto the polyurethane tube connecting the stainless steel cannula to the constant pressure head (refer figure 2.1). All air bubbles within this tube were expelled. Stiff tubing was used here, and for the pressure transducer connections (as necessary), to minimize any flow and pressure measurement errors from capacitive effects in the tube wall. The output of the flow probe was fed into a Transonic Systems (Ithaca, New York) HT101D ultrasonic flowmeter[iii]. Each of the pressure transducers was connected to a transducer amplifier on a Gould strip chart recorder, while the output of each transducer amplifier was fed into a Compaq portable type III computer. The output of the flow meter was simultaneously fed into the computer and the strip chart recorder.

The pelvic nerves were stimulated using a Grass stimulator. All stimulations were performed at 30 v, with a frequency of 50 Hz, and a pulse duration of 0.1 ms. Typically, the stimulation time was 10 s, although the effects of varying stimulation durations were investigated. The output of the stimulator was simultaneously fed into the computer and the strip chart recorder. Data, i.e. p_{ves}, p_{DU}, Q, the stimulation and the arterial pressure, were acquired at a frequency of 10 Hz.

The plane of anaesthesia and I.V. fluids were maintained during the full urodynamic analysis. The animal's heart rate and blood pressure were also continuously monitored.

[iii] This flow meter was specifically chosen because it provides an instantaneous flow rate measurement. Thus, no time delays between pressure and flow rate measurement are accrued, vastly simplifying the construction of a PQ curve.

During the filling phase of the experimental protocol, an (emptied) bladder was infused with 0.5% saline using a Harvard infusion pump at filling rates between 5 - 8 ml/min[iv]. A bladder capacity of 40 ml was used during each study since the best isometric pressures were obtained at this volume. Each urodynamic assessment was performed by stimulating the pelvic nerves, and recording the resulting intravesical pressures, distal urethral (DU) pressures, and urethral flow rates. Any post void residual volume was measured via the filling catheter, and also recorded.

The sphincter cuff was placed around the bladder neck only when an outlet obstruction was required. Before insertion, an effective zero cuff volume was created by completely evacuating the cuff of air. As a cuff was inflated or deflated, care was exercised to maintain an air tight seal.

The experimental protocol was conducted in two phases. The first phase involved the urodynamic assessment of a completely non-obstructed bladder. Typically, 5 - 6 urodynamic analyses were performed on an unobstructed bladder to estimate the reproducibility of the protocol, and obtain reference values for the outlet resistance and detrusor work parameters. In the (second) obstructed phase, the cuff was secured around the bladder neck, and inflated with 0.5 % saline in increments of 0.1 - 0.2 ml. After each incremental increase in cuff volume, a urodynamic assessment was performed to determine any changes in the parameters of interest (i.e. outlet resistance, and detrusor work). Inflation was continued until the bladder outlet was completely occluded, i.e. until a fully isometric contraction was obtained. The cuff volume was then incrementally decreased with urodynamic assessments at each incremental change. The reproducibility of the obstructed runs was established by comparing the pressures and flow rates between the ascending and descending steps of the phase 2 study at a constant cuff volume.

All catheters used for pressure measurements were flushed with 0.5% saline between successive run to ensure complete fluidic coupling between the pressure transducer, and point of pressure measurement.

[iv] Rates higher than this were found to provoke spontaneous bladder contractions.

3 Results and Discussion

The pressure flow data from each urodynamic assessment were reduced to a p_{det} vs Q^2 (bladder pressure vs. flowrate^2) plot. The data were also reduced to a Δp vs Q^2 plot, where Δp represents the difference between the detrusor pressure p_{det} and the distal urethral pressure p_{DU}.

$$\Delta p = p_{det} - p_{DU} \qquad (38)$$

The R value from the p_{ves} vs Q^2 relation, i.e. the effective urethral resistance estimate from the passive urethral resistance relation PURR, was termed the PURR resistance R_{PURR}. In the experimental setup, the outlet resistance seen by the contracting detrusor includes that presented by the urethral resistance proper as well as that generated

by the constant pressure head, stainless steel cannula, and the rigid connecting tube (refer Figure 2.1). To evaluate a pure urethral resistance, it is therefore necessary to subtract the effects of these "non-urethral" factors. A PURR is unsuitable for this since it is constructed using only p_{det} and Q data, and thus implicitly assumes all resistances are from the bladder outlet. The R value from the Δp vs. Q^2 curve however, by limiting itself to a resistance estimate between the bladder neck and the point of p_{DU} measurement, is more representative of a pure outlet resistance. Therefore, unless specified otherwise, any subsequent mention of urethral resistance will refer to that derived from the Δp vs. Q^2 relation, R_{DU}.

Each R value was constructed from the passive portion of the corresponding Δp vs. Q^2 curve by fitting a line (a first order polynomial) through the region of lowest resistance (i.e. the region of smallest slope). The intercept from the p vs Q^2 relation was equated to the minimum urethral opening pressure p_{muo} defined in the literature. (The reader is again reminded that the p_{muo} is a critical urethral closure pressure p_{cuc} as discussed in section 1.5).

The internal work, external active work, external passive work, and total work for each phase I and phase II study was computed using the relations presented in section 1.3.1.1. Additionally, the time to (urethral) opening t_o, the time to peak flow t_{Qmax} and the time from peak flow to the voiding terminus t_{zero} were evaluated. All times are referenced to the contraction initiation time $t=0$, and are schematically presented in Figure 1.10. The reader is encouraged to refer this diagram when reviewing the subsequent discussions involving these time parameters.

The results obtained from the male animals (i.e. animals #3 and #4 - refer Tables 2.1 and 3.1) showed very little reproducibility, and hence will not be presented in this section. The inconsistencies in these data may have resulted from a distortion of normal urethral flow patterns following the penile urethral transection. It is also possible that the male prostatic and membranous urethral segments utilized were not as robust as the corresponding female urethral length, and reacted more strongly to their invasion. Overall, the female animals presented significantly fewer surgical challenges. The data

from animal #1 (female) was discarded due to an experimental error incurred during the functional analysis. A functional analysis could not be performed on animal #7 (female) due to an acontractile bladder. Thus, only data from (female) animals 2, 5, 6, 8 and 9 will be considered in the following discussions (refer Table 3.1).

Animal	#1	#2	#3	#4	#5	#6	#7	#8	#9
Sex	F	F	M	M	F	F	F	F	F
Outcome	disc.	used	disc.	disc.	used	used	disc.	used	used

Table 3.1 Summary of the animal studies selected for presentation. The term "disc." is used to indicate those studies discarded due to the reasons presented in the preceding paragraph.

The females' lack of a prostate was not an issue since a sphincter cuff was used to model all outlet obstructions. In fact, using females simplified the interpretation of flow through the experimentally induced obstructions since females are immune to the BPH type occlusions that are sometimes present in their male counterparts.

3.1 Outlet resistance and detrusor dynamics

3.1.1 Outlet resistance

The outlet resistances computed using the Δp vs. Q^2 relation for the non-obstructed animals are presented in Table 3.2. As can be seen, significant variations are present. It would be convenient if these disparities could be assigned to some intrinsic

detrusor or urethral property that varies among animals. A property that definitely merits investigation in this context is the detrusor contractility. Detrusor contractility is clinically defined in terms of a peak isometric pressure p_{iso} and a total contraction duration.

	Resistance	$cmH_2O.s^2.ml^{-2}$			
Run	Dog 2	Dog 5	Dog 6	Dog 8	Dog 9
1	0.37 (0.95)	0.09 (0.96)	0.41 (0.99)	0.23 (0.97)	0.07 (0.93)
2	0.28 (0.96)	0.07 (0.97)	1.07 (0.98)	0.23 (0.97)	0.09 (0.90)
3		0.10 (0.98)	2.17 (0.96)	0.26 (0.99)	0.07 (0.99)
4		0.11 (0.96)	2.34 (0.99)	0.23 (0.94)	
5		0.13 (0.98)	2.46 (0.98)	0.35 (0.95)	
6		0.15 (0.95)			
7		0.14 (0.99)			
mean	0.32	0.12	1.69	0.26	0.076
std. deviation	0.06	0.03	0.90	0.05	0.012

Table 3.2   Reference outlet resistances under non-obstructive conditions. The R_{DU} was computed from the slope of the respective Δp vs. Q^2 relations. The correlation co-efficient (r^2) values from the corresponding linear regressions are included within parentheses.

In the experimental setup used, the total detrusor contraction duration is governed by the applied stimulation interval of 10 seconds (This stimulation time was maintained through all functional analyses since it represented the critical stimulation duration required to produce a maximum peak isometric pressure). Thus, for the purposes of this thesis, the single determinant of contractility is the peak isometric pressure. It should be noted at this juncture that the constant stimulation time forces an approximately constant total contraction duration (defined as the time period between the first increase in detrusor pressure - i.e. contraction initiation - $t=0$ and flow termination $t=t_{zero}$) for all experimental

runs in a *given* animal. It does not however mandate a constant total contraction duration over *all* animals. (The total contraction duration for a given stimulation will depend on intrinsic detrusor properties such as myocyte size and ATP stores that will vary from animal to animal). An appreciation of this difference is crucial to the understanding of both the behavior of the urethral time parameters (e.g. t_o) discussed shortly, and the shapes of the urethral tube laws presented in section 3.2.1.1.

Table 3.3 indicates that the peak isometric pressures (and the cuff volumes required to create an isometric obstruction) do vary among animals. Given the preceding discussion, this implies that detrusor contractilities also vary across animals. However, to implicate this as a source of outlet resistance disparity, a relation between the passive urethral resistance and the detrusor contractilities must exist. Such a relation is proposed below.

The passive urethral resistance is defined assuming the detrusor pressure p_{det} is proportional to the (flowrate)^2 (refer section 1.5). This relation is mathematically expressed in equation (34) as:

$$p_{det}(t)=p_{cuo}+RQ(t)^2 \qquad (34)$$

Considering that a hypertrophied bladder (albeit assuming functional myocytes and no fibrosis) will have a high contractility coupled to a low compliance and vice versa, one can postulate an inverse relation between the detrusor contractility and the detrusor compliance C_d. If this relation is now assumed linear, the following relations between the detrusor pressure p_{det}, bladder volume V, compliance C_d, and contractility can be defined:

$$C_d=\frac{dv}{dp_{det}} \qquad \text{and,} \qquad contractility=\frac{k}{C_d}=k\frac{dp_{det}}{dV} \qquad (39)$$

Dog	peak p_{iso} (cmH$_2$O)	cuff volume (ml)
2	37.4	1.2
5	48.5	1.5
6	48.9	1.3
8	34.6	1.1
9	43.9	0.8

Table 3.2   Detrusor contractility measured in terms of the peak isometric pressure p_{iso}. The cuff volume required to generate an isometric contraction is also indicated.

where k is an arbitrary constant of proportionality. By differentiating equation (34) with respect to Q, and using $Q = dV/dt$,

$$\frac{dp_{det}}{dQ}=2RQ(t)=2R\frac{dV}{dt} \qquad (40)$$

and by comparing equations (39) and (40),

$$k\frac{dp_{det}}{dV}=contractility=2kR\frac{dQ}{dt} \qquad (41)$$

Any variation in detrusor contractility can thus manifest as a variation in the outlet resistance and/or rate of change of flowrate dQ/dt. Thus, differences in contractilities must be considered when explaining the observed variation in non-obstructed outlet resistances.

Other physiologic factors such as variations in each animal's response to surgical

trauma may also be culpable. Experimental factors such as differences in the distance between the bladder outlet proper and the sphincter cuff, as well as the inadvertent stimulation of the urethra and/or bladder neck during the electrical stimulation of the pelvic nerves must also be examined in this context. Branches of the hypogastric nerves carrying a sympathetic nervous supply to the bladder neck and urethra travel within the pelvic nerves (with the parasympathetic supply responsible for the initiation of a bladder contraction). Any stimulation of the pelvic nerves may thus potentially trigger a sympathetic response in terms of a urethral and/or bladder neck contraction. The stimulation is also non-ideal in that the inherent conductivity of animal tissues make the localization of an electrical charge exclusively to the pelvic nerves impossible. Some diffusion of current to the adjacent urethral and bladder neck musculature, potentially triggering or potentiating their contraction must thus be expected. Any contraction of the urethra or bladder neck during a voiding contraction will produce inconsistencies in the computed outlet resistance. In fact, this phenomenon may well represent the major cause of outlet resistance variation between successive runs, at a constant obstructive degree, in a single animal.

Experimental errors in pressure and flow measurement present another source of resistance variation between animals, and between runs successive for a single animal. Pressure measurement errors merit special mention in this context. The pressure difference Δp required to construct the R_{DU} was computed by measuring the detrusor and distal urethral pressures individually, and then computing their difference (as opposed to directly measuring a difference). Any error in a single pressure measurement will thus be compounded in the Δp. This measurement error is however non-random, and can thus be assumed to remain constant through all runs during a given functional analysis. Such a constant pressure error should manifest itself purely as a shift of the Δp vs. Q^2 curve along the y (i.e. pressure) axis. Since the R_{DU} is computed from the slope of Δp vs. Q^2 curve, the R_{DU} should be relatively immune to this particular error. The major consequence of this error appears later, when attempting to use the Atkinson and Goldstein method to compute a urethral diameter, and is discussed in section 3.2.1.1.
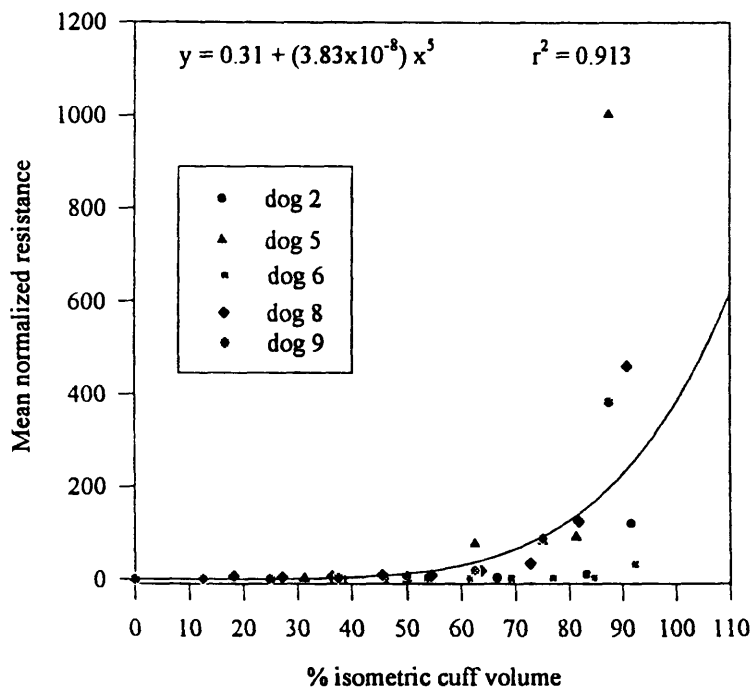
$$y = 0.31 + (3.83 \times 10^{-8})\, x^5 \qquad r^2 = 0.913$$

Mean normalized resistance

1200
1000
800
600
400
200
0

- • dog 2
- ▲ dog 5
- ■ dog 6
- ◆ dog 8
- ● dog 9

0 10 20 30 40 50 60 70 80 90 100 110

% isometric cuff volume

Figure 3.1   The response of the mean bladder outlet resistance to varying outlet obstructions. All resistances are computed from the slope of a Δp vs Q^2 curve.

The bladder outlet resistance response to the cuff induced obstructions is somewhat as expected - an increase in obstruction produces an increase in resistance (refer Figure 3.1). The overall response pattern is however non-linear. Figure 3.1 thus implies that the sphincter cuff can effectively function only in the realms of complete obstruction or no/minimal obstruction. Therefore, the sphincter cuff, as used in this protocol, is unsuitable for chronic studies attempting to model the temporal behavior of a BPH type obstruction which gradually progresses from mild to moderate to severe. The cuff is however effective at modeling the extremes of obstruction, with the transition from a mild/minimal obstruction to a severe obstruction occurring at approximately 75% of the isometric cuff volume.

The time to commencement of flow or time to urethral opening t_o (measured from the contraction initiation point $t=0$) is observed to increase with increasing outlet obstruction (refer figure 3.2). This can be explained in several alternate ways. For example, one could imagine that if the detrusor functioned along a fixed power curve (even after the introduction of an outlet obstruction), the time required for that detrusor to

raise the intravesical pressure high enough to initiate flow will increase with an increasing outlet obstruction. (The detrusor remaining on the same power curve implies an absence of detrusor compensation to the increased outlet resistance). Alternately, one can imagine the detrusor functioning on successively higher power curves as outlet obstruction is increased (i.e. actively compensating), but being unable to compensate sufficiently for the increased resistance, and thus producing increased opening times t_o that are however smaller than the t_o increase under non-compensatory conditions. Thus, all that can be definitely inferred from the results in Figure 3.2 is that if any detrusor compensation occurs with increasing outlet obstruction, it is not 100% efficient (in terms of maintaining a constant t_o).
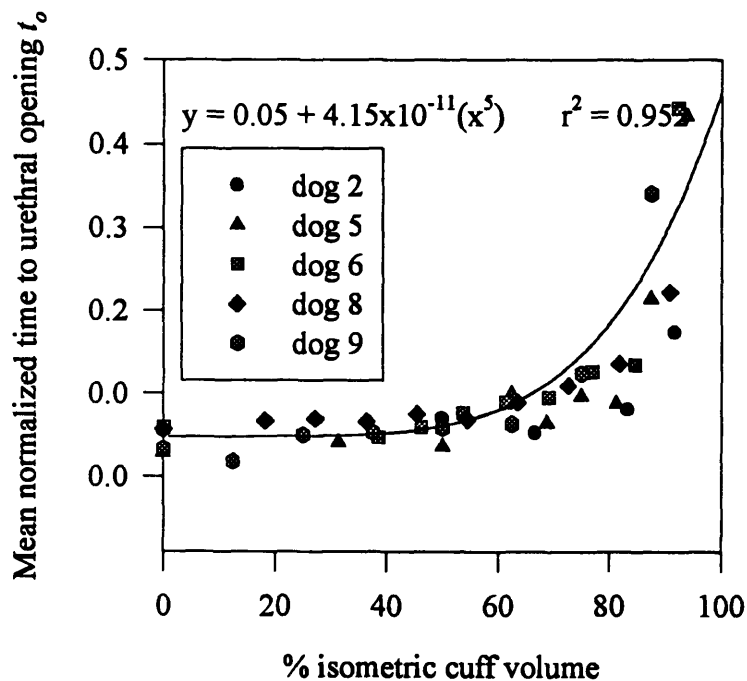

Figure 3.2   Response of the time to flow commencement (i.e. time to urethral opening t_o) to varying outlet obstructions. All data are normalized by the corresponding total contraction times.

3.1.2   Power and energy considerations

As defined in section 1.3.1.1, the external work refers to the work incurred during micturition that can be measured in terms of a detrusor pressure p_{det} and flowrate Q. This thesis will used the term *active* work to describe the detrusor external work expended between non-voiding and peak flow conditions (i.e from t_o to t_{Qmax}). Physiologically, this work represents the detrusor flow work done during the time required for the flow controlling zone *fcz* to relax from its completely closed state - zero flow, to its completely relaxed state - peak flow (refer Figure 3.6). The term *passive* work is similarly used to describe the detrusor flow work expended between peak flow and the voiding terminus (i.e. from t_{Qmax} to t_{zero}). Although the term "passive" is used for this work component, it should not be misconstrued as implying the bladder is acontractile from t_{Qmax} to t_{zero}. Rather, the term "passive" refers to the urethral flow control zone *fcz*, and is used to illustrate that the *fcz* has fully opened and is relaxed during this period. The passive work thus physically represents the work expended by a detrusor in propelling flow through a fully relaxed "urethra" (refer Figure 3.8).
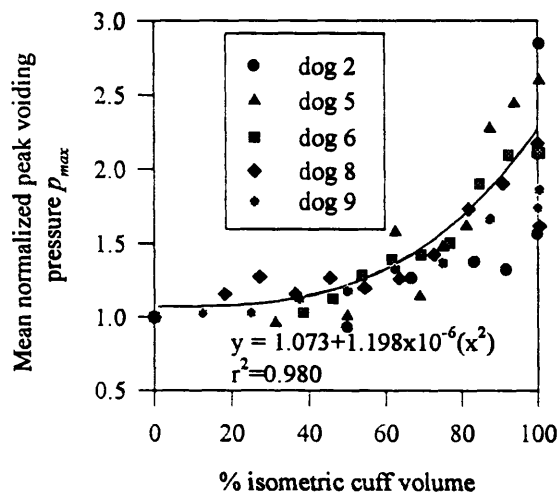

Figure 3.3   The response of the peak voiding pressure to a varying outlet obstruction. All pressures are normalized by the corresponding averaged peak non-obstructed voiding pressure.
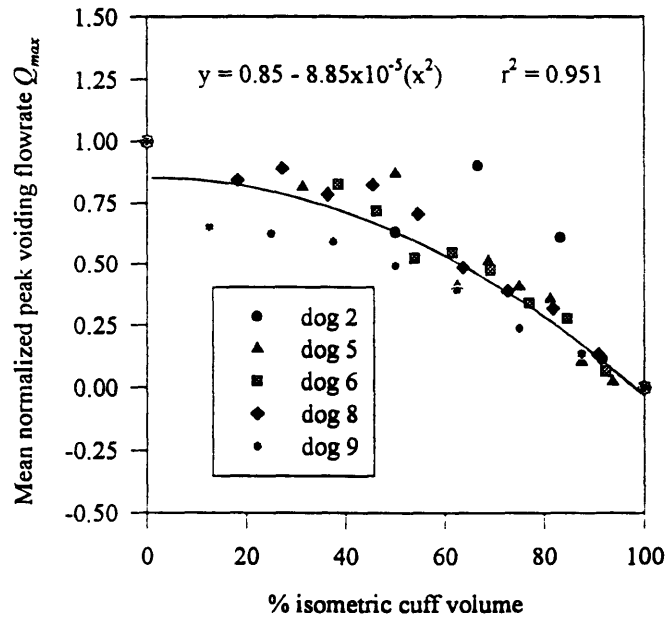
Figure 3.4 The response of the peak flowrate Q_{max} to a varying outlet obstruction. All data are normalized by the corresponding averaged peak non-obstructed peak flowrate.
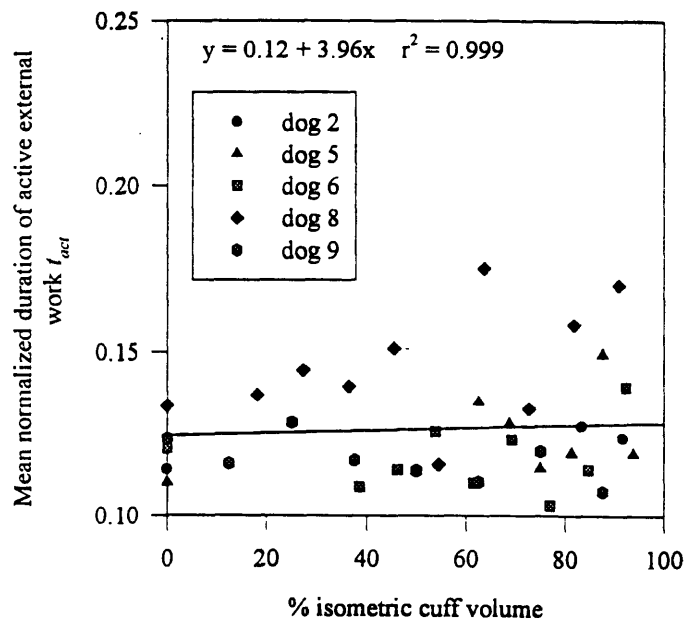

Figure 3.5 The response of the active external work duration t_{act} (i.e. $t_{Qmax} - t_o$) to varying outlet obstructions. All data are normalized by the respective total contraction duration.

As indicated in equation (13), the external work is computed in terms of a voiding pressure p_{det}, flowrate Q, and contraction duration t.

$$W_{ext} = \int P_{det}(t)Q(t)dt \qquad (13)$$

For the active external work, the contraction duration t_{act} is equal to the time between urethral opening t_o and peak flow t_{Qmax} ($t_{act} = t_{Qmax} - t_o$). Clinically, the active contraction time has been shown to increase with increasing outlet obstruction. However, Figure 3.5 indicates that experimentally, the active contraction duration remained approximately constant with increasing obstruction. This is most likely an artifact of the bladder stimulation. In general, the time to peak flow t_{Qmax} occurred within 4 - 5 seconds of flow commencement, and thus within the stimulation interval of 10 seconds. It is thus conceivable that the stimulation duration forces the active contraction time to remain fixed independent of any changes at the bladder outlet.

Given this approximately constant active contraction duration t_{act}, the active external work reduces to a function of only the voiding pressure p_{det} and flowrate Q. As discussed in section 1.5, the voiding pressures are expected to increase, and flowrates expected to decrease with increasing outlet obstruction. This result is confirmed in Figures 3.3 and 3.4. Figure 3.6 indicates that the active external work decreases with increasing outlet obstruction. This implies that the increase in voiding pressures cannot compensate for the drop in flowrates as the outlet obstruction severity is increased from 0% to 100%.

As discussed previously, for a given animal, the stimulation duration will hold the total contraction time approximately constant. The time to opening t_o, the active contraction duration t_{act}, and the passive contraction duration t_{pas}, the sum of which must equal the total contraction time, are thus constrained to vary within a constant window. It has already been shown that the time to opening t_o increases with increasing outlet obstruction (Figure 3.2). Since the active contraction duration t_{act} remains approximately constant with increasing obstruction, it can thus be expected that the passive contraction

$$y = 0.90 - (1 \times 10^{-10}) x^5 \quad r^2 = 0.887$$

Legend:
- dog 2
- dog 5
- dog 6
- dog 8
- dog 9

Axes: Mean normalized active external work (vertical), % isometric cuff volume (horizontal)
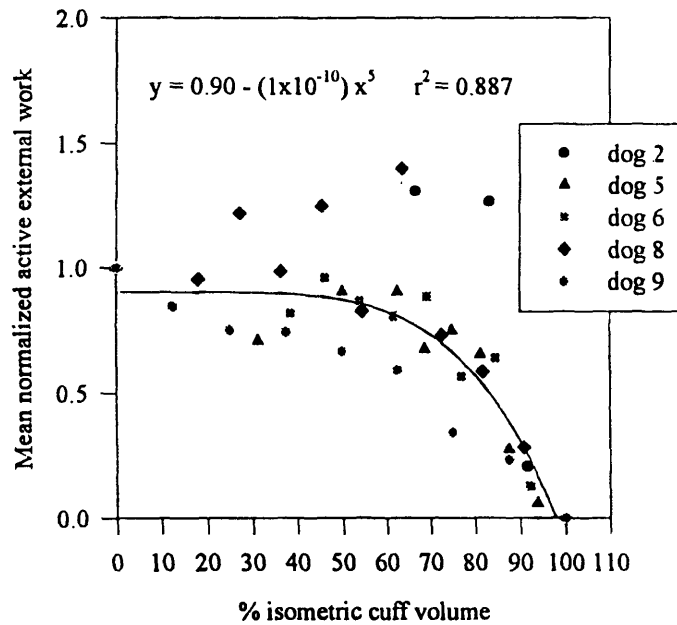
Figure 3.6 Response of the active external work to a varying outlet obstruction. All data are normalized by the mean active external work under non-obstructive conditions.
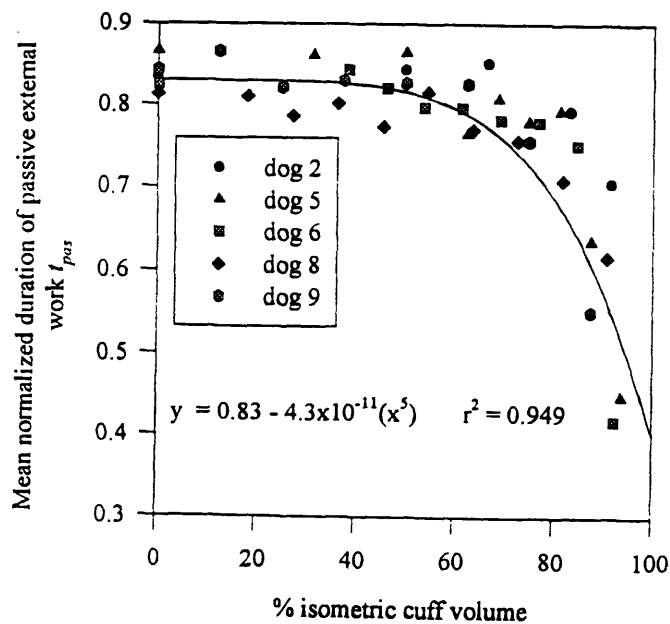

$$y = 0.83 - 4.3 \times 10^{-11} (x^5) \quad r^2 = 0.949$$

Legend:
- dog 2
- dog 5
- dog 6
- dog 8
- dog 9

Axes: Mean normalized duration of passive external work t_{pas} (vertical), % isometric cuff volume (horizontal)

Figure 3.7 Response of passive contraction duration t_{pas} (i.e. $t_f - t_{Qmax}$) to varying outlet obstructions. All data are normalized by the corresponding mean total contraction duration.

duration t_{pas} (defined as the difference between the total contraction time t_f and the time to peak flow t_{Qmax}, i.e. $t_{pas} = t_f - t_{Qmax}$) will decrease with increasing obstruction. This is confirmed in Figure 3.7.
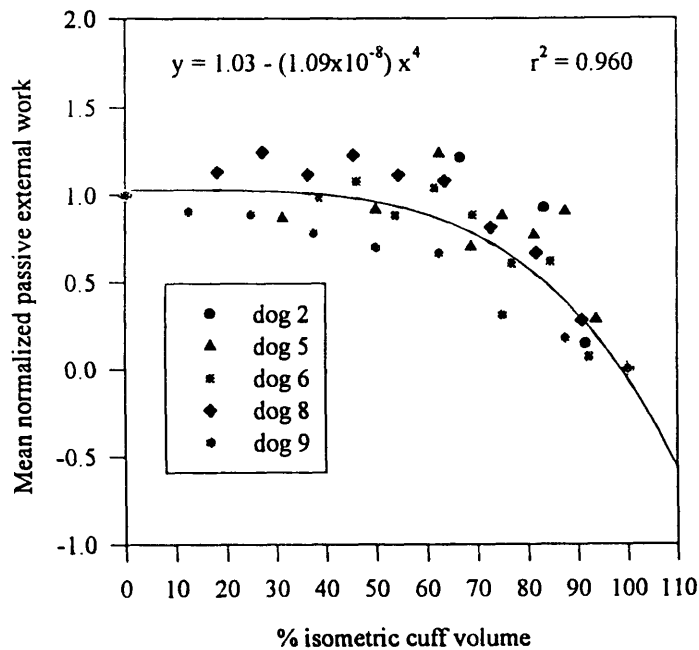

Figure 3.8   The response of the passive external work to varying outlet obstructions. All data are normalized using the mean passive external work under non-obstructive conditions.

Since the voiding pressures, flowrates and contraction durations defining a passive external contraction change with outlet obstruction, they must all be considered when evaluating the passive work response to outlet obstruction. In this context, Figure 3.8 shows that with respect to the passive work, the increase in voiding pressures with increasing obstruction cannot compensate for the concomitant decreases in flowrate and contraction duration.

The total external work is defined as the sum of the external active work and the external passive work. The reader is reminded that this total external work (and, even the active and passive components of the total external work individually) can be related to

the flow kinetic energy as discussed in section 1.3.1.1.

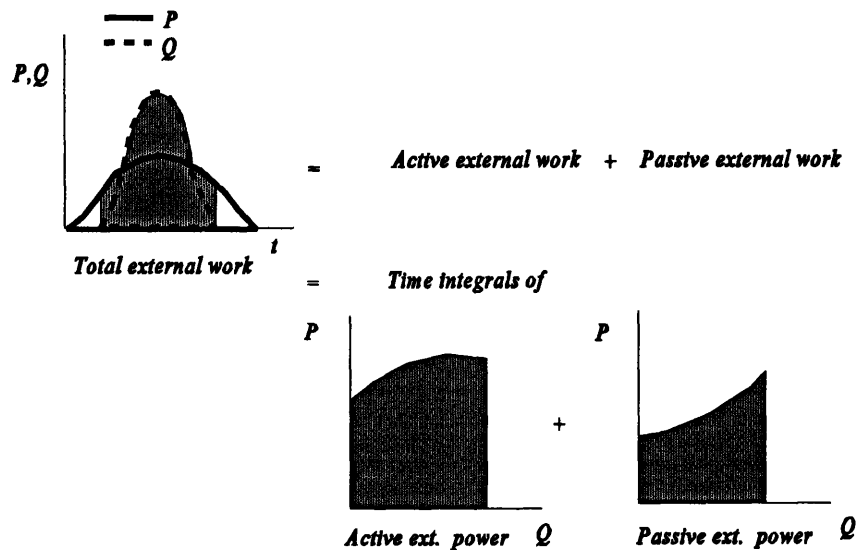$$W_{total.external} = W_{active} + W_{passive} \qquad (42)$$

Figure 3.9 Schematic representation of the components of the total external work, and their relation to the pressure-flow (PQ) curve. The areas shaded correspond to the work parameters of interest.

Given equation (42), and that both the external active work (Figure 3.6) and the external passive work (Figure 3.8) decrease with increasing outlet obstruction, the result shown in Figure 3.10 with the total external work decreasing as the outlet obstruction is increased is as expected.

It should be noted that the total external work can be defined in terms of the volume integral $\int pdV$. Considered in this form, and given that the detrusor pressures increase with increasing obstruction, the total external work will decrease with obstruction only if the volumes voided during a contraction also decrease with obstruction. Given the constant total contraction duration, and the identity $V = \int Qdt$, this requirement of a decreasing voided volume is equivalent to requiring a decrease in the voiding flowrates

with obstruction.   This has been established in Figure 3.4.

$$y = 0.99 - (1.05 \times 10^{-8})\, x^4 \qquad r^2 = 0.952$$

Figure 3.10   Response of the total external work to varying outlet obstructions. All data are normalized by the corresponding total external work under non-obstructive conditions.

$$y = 1.124 + (5.436 \times 10^{-6})\, x^3 \qquad r^2 = 0.978$$

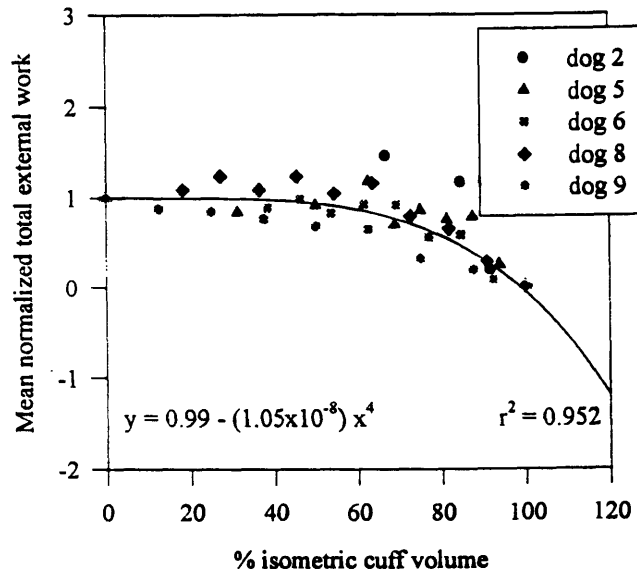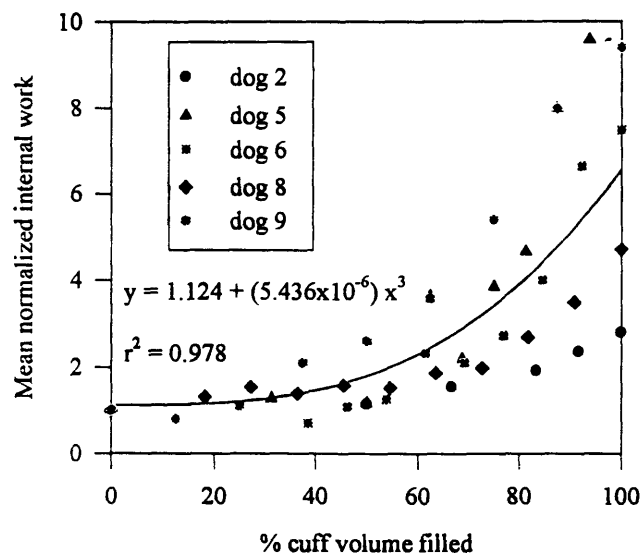**Figure 3.11**   The response of the internal work to a varying outlet obstruction. All data are normalized by the corresponding internal work under non-obstructive conditions.

The internal work (i.e. the work required to serially elongate the elastic elements of the detrusor wall), to a first approximation, is defined in terms of a pressure difference, and bladder capacity (refer equation (15) and its proceeding discussion). Since a constant bladder capacity was maintained through all functional analyses, the internal work will depend purely upon the pressure difference ($p_v - p_o$), where p_v and p_o are the detrusor pressures at flow commencement, and baseline respectively (refer equation (17)).

This pressure difference is identical to the critical urethral opening pressure p_{cuo} discussed in relation to the PURR, and will be equal to the minimum urethral opening pressure p_{muo} if a perfectly elastic urethra is assumed (refer section 1.5). Given this formulation with a constant baseline pressure (as was maintained experimentally), any change in the p_{cuo} will translate into a proportional change in the internal work and vice versa. For this reason, the response of the p_{cuo} to outlet obstruction will not be explicitly presented.

Since the internal work increases with increasing outlet obstruction, it can be inferred that the p_{cuo} has increased with increasing outlet obstruction (with the increase in the p_{cuo} causing the increase in the internal work). This increase in the internal work is also related to the increase in the time to urethral opening t_o with increasing outlet obstruction (refer Figure 3.2), since t_o is the duration of the internal work.
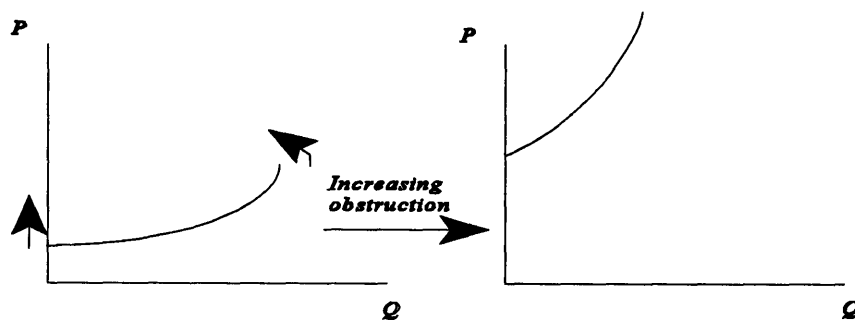

Figure 3.12a Expected change in the PURR from a BPH type obstruction showing compressive and constrictive characteristics.

Further, this result, in conjunction with that shown in Figure 3.1 (an increasing outlet obstruction producing an increasing outlet resistance) implies that the sphincter cuff creates an outlet obstruction exhibiting both compressive and constrictive characteristics (refer Figure 1.15). In this context, the sphincter cuff functions similar to a BPH type outlet obstruction.

The total work (refer equation (11)) is defined as the sum of the total external work and the internal work. This definition however implicitly assumes that losses during a voiding cycle are negligible (If losses cannot be ignored, the total detrusor work is composed of the sum of the internal work, the total external work, and the losses). Fluidic losses can be induced by both viscous effects (laminar flow through the narrowings, widenings and bends of a urethra), and by inertial effects (turbulence). Such losses have however been characterized as minor[4]. Equation (11) will thus be assumed an adequate representation of the micturitional energy balance.
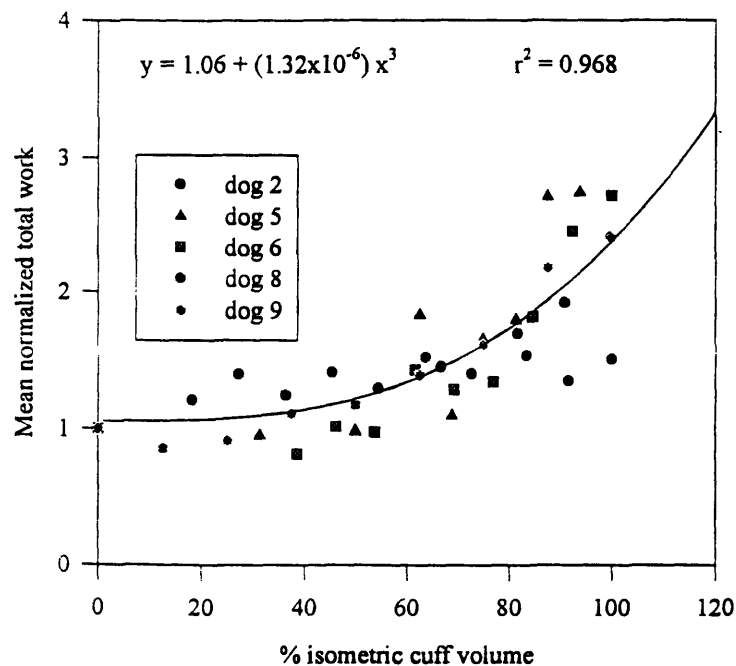

Figure 3.12 The response of the total detrusor work to a varying outlet obstruction. All data have been normalized by the corresponding mean unobstructed total work.

Figure 3.12 indicates that the total detrusor work increases with an increasing outlet obstruction. Given that the internal work increases with increasing obstruction (Figure 3.11) while the external work decreases with increasing obstruction (Figure 3.10), this implies that the internal work component dominates the total work. This becomes very evident when examining Figure 3.13 which shows the total detrusor work at each cuff volume explicitly divided into its internal and external components. Figure 3.13 also indicates that as the severity of an outlet obstruction is increased, the total work output of the bladder will increase until the total work is identical to the internal work at zero flowrate.
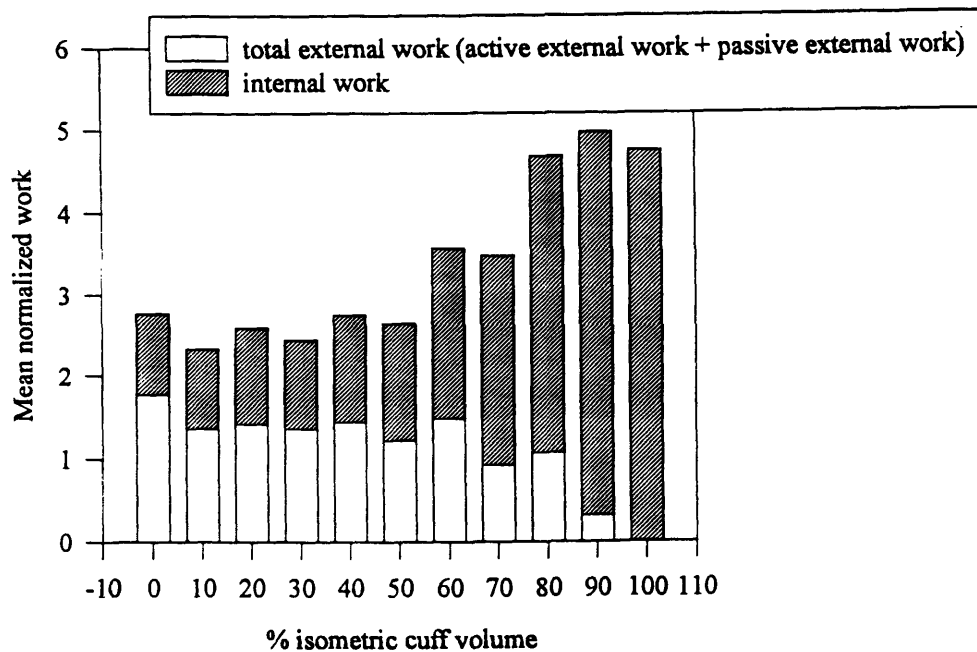
Figure 3.13 A bar graph representation of the total detrusor work. Here, the internal and external work components of the total work are explicitly presented together. All internal and external work values are normalized with respect to the corresponding mean non-obstructed value.

This maximum will occur at a purely isometric contraction - During an isometric contraction the change in bladder volume is zero ($dV = 0$) yielding zero $\int pdV$ (external) work. Thus, all work during an isometric contraction must be of the internal variety.

Experimentally, this maximum total work (or, equivalently the maximum internal work) is governed by the electrical energy of the stimulus. Under normal physiologic conditions, however, the stored biochemical energy is the limiting factor (refer the discussion on smooth muscle contraction in section 1.3.1.1).

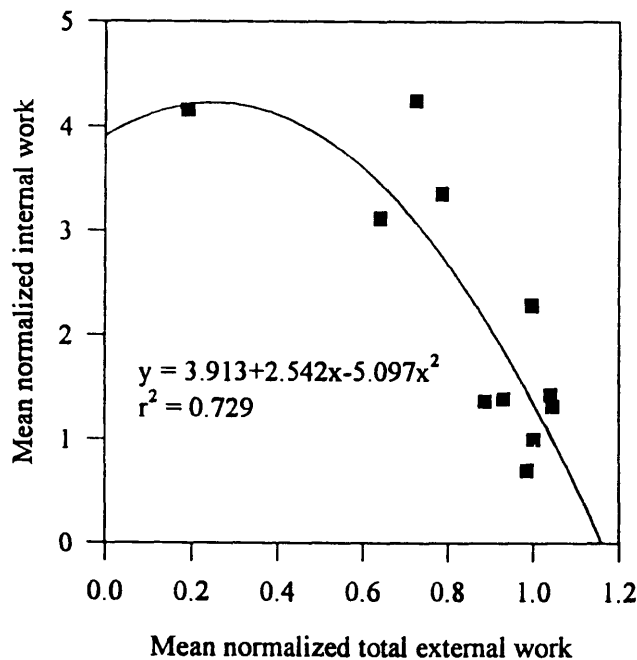The graph shows a plot with Mean normalized internal work on the y-axis (0 to 5) and Mean normalized total external work on the x-axis (0.0 to 1.2). The fitted curve equation is:

$$y = 3.913 + 2.542x - 5.097x^2$$
$$r^2 = 0.729$$

Figure 3.14 The relation between the total external work (i.e. external active work + external passive work) and the internal work with increasing outlet obstruction.

Figure 3.14 demonstrates a negative correlation between the internal and external work with increasing obstruction (also indicated, albeit qualitatively, in Figure 3.13). This implies that as the severity of an outlet obstruction is increased, the fraction of the total work required to elevate the detrusor pressure over the critical urethral opening pressure p_{cuo} (i.e. the detrusor work required to initiate flow - the internal work), increases with respect to the fraction of the total work required to propel flow through the urethra (the external work).

The preceding results can also be used to compare the sensitivities of two independent parameters in detecting changes in outlet obstruction. The resistance computed from the Δp vs Q^2 can be contrasted to the internal work in this context. As

shown in Figure 3.15, the correlation between these two parameters is exponential, with the internal work changing rapidly (with relatively smaller changes in the outlet resistance) at low outlet obstructions. Thus, at low obstructions, the internal work appears to be the more sensitive parameter. At moderate levels of obstruction, however, the internal work begins to saturate, and the rates of change of both parameters become approximately equal. At very high obstructions, the internal work has saturated and only the outlet resistance will change. The clinical implications of this result will be discussed in section 4.

$$y = 3.34(1-e^{-0.03x}) + 0.86$$

$$r^2 = 0.967$$

(y-axis: Mean normalized internal work, x-axis: Mean normalized resistance)

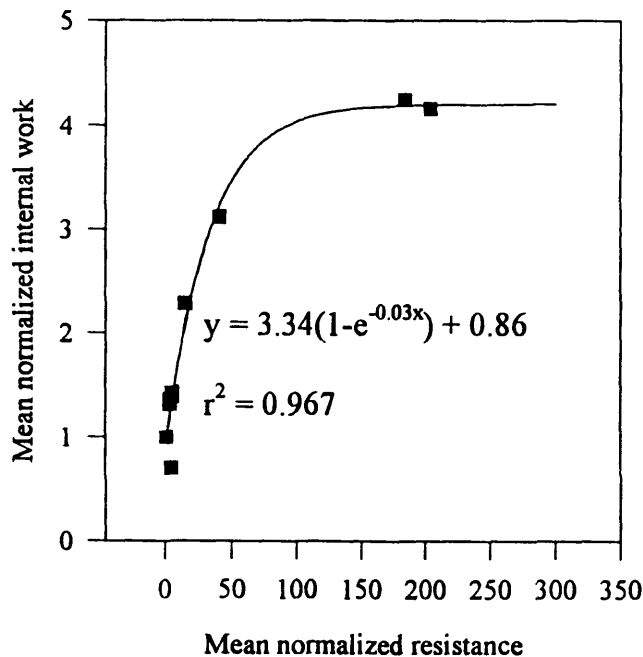**Figure 3.15** The correlation between the internal work and the passive urethral resistance as computed from the Δp vs. Q^2 relation.

A correlation between the total external work and the passive resistance can similarly be assessed. This relation is presented in Figure 3.16. As with the internal work, the external work changes rapidly at low obstructions and saturates as the obstruction is increased.
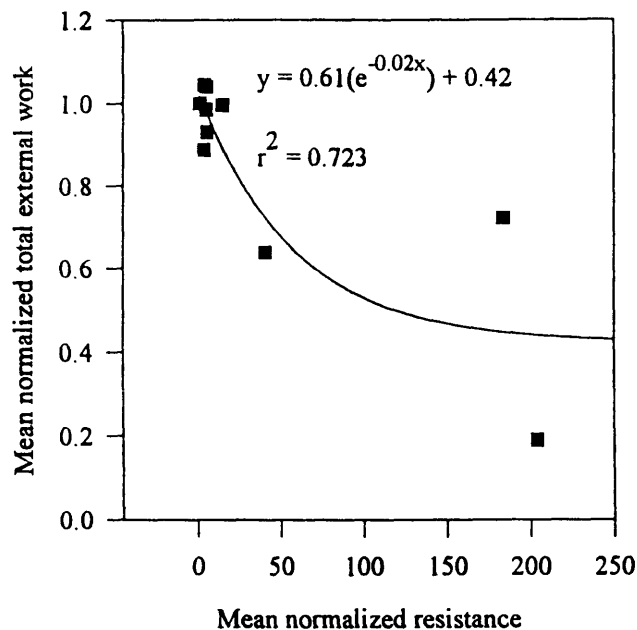
The chart shows data points with the fitted equation:

$$y = 0.61(e^{-0.02x}) + 0.42$$

$$r^2 = 0.723$$

Y-axis: Mean normalized total external work, ranging 0.0 to 1.2
X-axis: Mean normalized resistance, ranging 0 to 250

Figure 3.16 The correlation between the total external work (i.e. external active work + external passive work) and the passive urethral resistance as computed from the Δp vs. Q^2 relation.

Since the total work is composed of the sum of the internal and external work, and since the correlation of these "component" parameters to the passive urethral resistance is known, the explicit correlation between the total work and the urethral resistance will not be considered here[i].

3.2 Characterization of urethral flow

Tubular flows, regardless of the specific characteristics of the tube (rigid/distensible) can exist in three alternate regimes: inviscid, laminar or turbulent. The

---

[i] Since it has been established that the internal work dominates the total work, one can in fact expect this correlation to closely mirror that between the internal work and the passive urethral resistance.

inviscid regime is a highly idealized condition, and describes a fluid with zero viscosity μ.
Nonetheless, many flows can be approximated as inviscid if both the rate of shear
deformation $\dot{\gamma}$ and viscosity of the fluid particles are small. This can be seen as follows:
Consider a viscous flow through a tube of radius $r=a$. The fluid viscosity μ mandates a no
slip condition which constrains all fluid particles at the tube wall ($r=0$) to stick to the
surface, and thus have a zero velocity. Further, if incompressible flow is assumed, the
conservation of mass requires that a constant flowrate Q be maintained throughout the
flow length (refer equation (5)). Thus, if fluid is retarded peripherally (and a constant flow
cross sectional area a is assumed), the central fluid core must accelerate such that the
product $vA = Q$ remains a constant and mass is conserved. This results in a velocity
profile as shown in Figure 3.17a, with radially increasing velocities v ($dv(r)/dr>0$), and
$v=0$ at $r=0$[ii]. If one now considers the fluid chunk at time t, as shown in Figure 3.17b,
the condition $dv(r)/dr>0$ implies that within an incremental time δt, the top of the chunk
will be displaced relative to the bottom. The relative velocity difference v_{rel} between the
top and the bottom of the fluid chunk causing this displacement can be estimated as:

$$v_{rel} \approx (v + \frac{\partial v}{\partial r}\delta r) - v = \frac{\partial v}{\partial r}\delta r \qquad (43)$$

The distance the top of the chunk moves relative to the bottom δd in the time δt
can now be calculated as:

$$\delta d = v_{rel}\delta t = \frac{\partial v}{\partial r}\delta r \delta t \qquad (44)$$

The shear rate $\dot{\gamma}$ is defined as the rate of change of the angle of deformation $\delta\phi$.

$$\dot{\gamma} = \frac{d\phi}{dt} \qquad (45)$$

[ii] Since flow is continuous, a velocity profile will also be continuous.
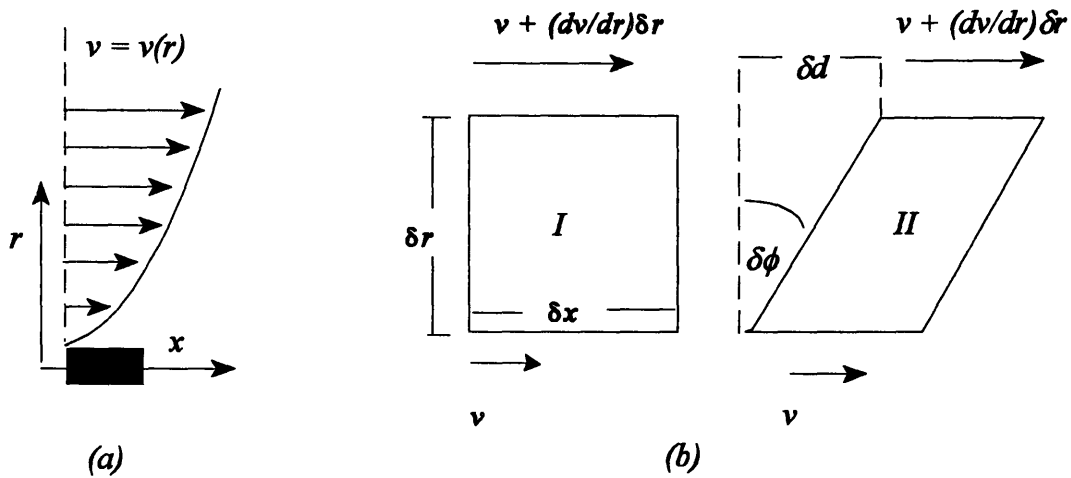
Figure 3.17 (a) a segment of a typical tubular velocity profile and (b) an infinitesimally small chunk of fluid under deformation by shear stresses at time $t=0$ (I) and time $t=t+\delta t$ (II).

Since this angle of deformation $\delta\phi$ is small for a small time increment δt,

$$\delta\phi \approx \tan(\delta\phi) = \frac{\delta d}{\delta r} = \frac{\partial v}{\partial r}\delta t \tag{46}$$

and from equations (45) and (46),

$$\dot{\gamma} = \frac{\partial v}{\partial r} \tag{47}$$

The fluid shear stress τ can now be defined in terms of the shear rate and viscosity μ as:

$$\tau = \mu\dot{\gamma} \rightarrow \tau = \mu\frac{\partial v(r)}{\partial r} \tag{48}$$

Thus, with viscosity, each particle in a flow field will be subjected to a shear stress τ and a corresponding shear deformation (refer Figure 3.17b). Equation (48), confirms that shear stresses can be ignored (i.e. $\tau \sim 0$, and inviscid flow can be assumed) if either the fluid viscosity μ and/or the shear rate are negligible. Physically, shear stresses retard relative motion between fluid particles (as friction retards the relative motion of solids). If the relation between the shear stress and shear rate of a fluid is linear (i.e. if the viscosity μ is a constant), the fluid is referred to as a Newtonian fluid.

Note that Figure 3.17 assumes that the horizontal borders of the fluid chunk remain parallel to the x axis (i.e. $v = v(r)$) a more generalized formulation of the shear rate would allow the velocity to change in both the x and r directions (two dimensional flow), with the velocity $V(x,r) = u(x,r) + v(x,r)$ where u and v are the velocity components in the x and r directions respectively. The shear rate then becomes[14]:

$$\dot{\gamma} = \frac{1}{2}(\frac{\partial v}{\partial r} + \frac{\partial u}{\partial x}) \qquad (49)$$

The relation between the shear rate, viscosity and shear stress (refer equation (48)) however remains unchanged.

In laminar flow, at least one of the velocity gradients ($\partial v/\partial r$ or $\partial u/\partial x$) is non-zero. The term laminar is used since this flow appears as a series of thin fluid sheets (laminae) sliding over one another. Because of this orderly motion, in laminar flow, fluid particles move along fixed streamlines with almost no lateral mixing. Once fully developed conditions are attained (i.e. once the velocity profile becomes fixed - a parabola in tube flow, as will be discussed later), the flow velocity will remain constant in time, although varying in space.

A turbulent flow is characterized by random fluctuations in fluid velocity (i.e. velocity is now dependent on time and space). These velocity fluctuations lead to an intense mixing of fluid particles causing small lumps of fluid (termed eddies) to be thrown around during flow. Because each of these lumps carry mass, and thus momentum and

energy, the rates of momentum transfer (causing an apparent shear stress τ_{app}), of heat transfer and the rate of mixing of dissimilar fluids are extremely high in turbulent flow. Inertial effects (in terms of a mass transfer) thus dominate the characteristics of turbulent flow whereas viscous effects dominate laminar flow. If a turbulent velocity V is defined in terms of a time averaged velocity component $<V>$ and a fluctuating component V', with $V = <V>+V'$, the apparent stresses τ_{app} generated by a momentum transfer (also referred to as turbulent or Reynold's stresses) can be described in terms of V' and the fluid density ρ. If a two dimensional flow is assumed (i.e. $V = v(x,y,t)+u(x,y,t)$), the apparent shear stresses τ_{app} are[15]:

$$\tau_{app} = -\rho u'v' \qquad (50)$$

A mixing length model can be used to approximate the component velocity fluctuations (u',v') in terms of their respective time averaged velocities ($<u>$ and $<v>$) as follows:

$$u' \approx -l(\frac{\partial <u>}{\partial r}) \qquad \text{and} \qquad v' \approx -u' \approx l(\frac{\partial <u>}{\partial r}) \qquad (51)$$

where, l represents the fluid mixing length. The apparent shear stress τ_{app} thus becomes (contrast with the viscous shear stress τ - equation (48)):

$$\tau_{app} = \rho l^2 (\frac{\partial <u>}{\partial y})^2 \qquad (52)$$

The inertial forces influencing fluid particles can be estimated as the product of a dynamic pressure p_{dyn} and area A. The dynamic pressure in turn can be approximated in terms of the local velocity V as:

$$p_{dyn} = \frac{1}{2}\rho V^2 \qquad (53)$$

The area A can be approximated as the square of a reference length l. Thus, the inertial force $F_{inertial}$ can be estimated as:

$$F_{inertial} \sim \rho V^2 l^2 \qquad (54)$$

The viscous shear stress affecting fluid particles is defined in equation (48). The derivative $\partial v(r)/\partial r$ in this equation can be approximated by considering the velocity change from the fluid-tube interface ($v=0$) to a velocity V occurring over a reference length l.

$$\frac{\partial v}{\partial r} \approx \frac{\Delta v}{\Delta r} \sim \frac{V-0}{l} = \frac{V}{l} \qquad (55)$$

The shear force F_{shear} is equal to the product of the shear stress τ and a reference area $A = l^2$. Thus, combining equations (48) and (55), the shear force F_{shear} can be estimated as:

$$F_{shear} \sim \mu(\frac{V}{l})l^2 = \mu V l \qquad (56)$$

The ratio of the $F_{inertial}$ to the F_{shear} provides an estimation regarding the relative importance of inertial vs. viscous effects in a given flow field. This ratio is termed the Reynold's number R_e, and can be derived as follows:

$$\frac{F_{inertia}}{F_{shear}} \sim \frac{\rho V^2 l^2}{\mu V l} = \frac{\rho V l}{\mu} = R_e \qquad (57)$$

Since as discussed previously, viscous effects dominate laminar flow, and inertial

effects dominate turbulent flow, the Reynold's number thus essentially defines when each flow condition can be assumed. This is discussed in greater detail below.

It should be noted that laminar flow can become turbulent through a poorly understood process termed transition. Transition can occur naturally at high flowrates, and can be precipitated by the introduction of flow disturbances (e.g. increased roughness at a fluid-solid interface).

3.2.1   The Reynolds number

The characteristics of laminar and turbulent flows were first introduced by Osborne Reynolds in 1883, when he experimentally showed that the precise nature of a pipe flow is dependent on the dimensionless Reynolds number R_e defined in equation (57). For tube (or pipe) flow, the tube diameter D is substituted for the characteristic length l used in this expression. The Reynolds number for tube flow thus becomes:

$$R_e = \frac{\rho VD}{\mu}$$

(58)

Experimentally, Reynolds found that laminar flows typically existed at R_e values below 2000, whereas turbulent flows existed at higher R_e values. He also discovered that the exact point of transition from the laminar to the turbulent regime depended on experimental conditions such as background vibrations and other flow disturbances.

Modern fluid dynamics has condensed these results to approximately define the thresholds of laminar and turbulent flows. Here, a Reynolds number of 4000 is considered a minimum for the presence of turbulent flow, while flows with Reynolds numbers of up to 2300 are considered laminar. Reynolds numbers between the limits of 2300 and 4000 are considered non-specific, defining unpredictable flows which may rapidly fluctuate between the laminar and turbulent regimes.

As shown in equation (57), the Reynolds number can be physically interpreted as a ratio indicating the relative importances of inertial and viscous forces in a given flow field. Strictly speaking, any Reynolds number greater than 1 indicates that inertial effects are greater than viscous effects in the corresponding flow. However, the reader should note that the upper limit for laminar flow is a Reynolds number of 2300, and that by definition, viscous effects dominate laminar flow. The fundamental characteristics of laminar and turbulent flow are tabulated below.

Characteristic	Laminar flow	Turbulent flow
Reynolds number	< 2300	> 4000
Stream lines	rectilinear	chaotic, eddies
Entrance length[†]	$\sim 0.06 R_e d^*$	$\sim 4.4 d^* R_e^{1/6}$ (small dependence on R_e)
Pressure loss	$(128 \mu l Q)/(\pi d^4)$	$\sim (\rho l Q^2)/d^5$
Lateral mixing	small	large

† Defines the tube length required for the emergence of fully developed flow. Although the concepts of developed and entry length flow are discussed subsequently, the entry length formulae were introduce here for completeness.
* Tube diameter.

Table 3.3 Summary of laminar and turbulent flow characteristics.

It should be noted that the pressure loss in laminar flow is proportional to the flowrate Q, while the pressure loss in turbulent flow is proportional to the (flowrate)^2. Also, the losses in both regimes are very strongly dependent on the tube radius r.

From the preceding discussion, it is clear that the computation of a Reynolds number is pivotal to any description of urethral flow. As shown in equation (58), the Reynolds number is defined in terms of two "generic" parameters that can be referred (the fluid density ρ and viscosity μ), and two parameters specific for the system under consideration (the tube diameter D, the flow velocity V) that must be measured.

Experimentally, however, only the detrusor pressure p_{det}, the distal urethral pressure p_{DU}, the urethral length l between these two points of pressure measurement, and flowrate Q were measured. Therefore, given that the flowrate is defined as the product of a flow velocity V and tube cross sectional area A (or, alternately the tube diameter D, with $Q = VA = V\pi D^2/4$), and no explicit velocity or diameter measurement was made, it was not possible to compute values for a V and a D using the measured flowrate Q. It was thus not possible to directly use equation (58) in computing the Reynolds number. An alternate approach as described by Atkinson and Goldstein[16] was used in this context, and is described below.

3.2.1.1   Flow in the inlet length of a circular pipe

The proceeding discussion is adapted from *Modern Developments in Fluid Dynamics*, S. Goldstein (Ed), Dover Publications, New York, pp 299-309, 1965. An expression for the pressure drop Δp between two points along a fluid stream can be estimated starting from the equations of motion, assuming symmetry of flow about the tube axis, with u and v representing, the axial and radial components of the flow velocity respectively.

$$u\frac{\partial u}{\partial x}+v\frac{\partial u}{\partial r}=-\frac{1}{\rho}\frac{\partial p}{\partial x}+\nu(\frac{\partial^2 u}{\partial r^2}+\frac{1}{r}\frac{\partial u}{\partial r}+\frac{\partial^2 u}{\partial x^2})$$

(59)

$$u\frac{\partial v}{\partial r}+v\frac{\partial v}{\partial r}=-\frac{1}{\rho}\frac{\partial p}{\partial r}+\nu(\frac{\partial^2 v}{\partial r^2}+\frac{1}{r}\frac{\partial v}{\partial r}-\frac{v}{r^2}+\frac{\partial^2 v}{\partial x^2})$$

(60)

The equation of continuity is defined by:

$$\frac{\partial(ru)}{\partial x}+\frac{\partial(rv)}{\partial r}=0$$

(61)

And, since the stream function ψ must identically satisfy the continuity equation, a stream function $\psi(x,r)$ exists such that,

$$u = \frac{1}{r}\frac{\partial \psi}{\partial r} \qquad \text{and,} \qquad v = -\frac{1}{r}\frac{\partial \psi}{\partial x} \qquad (62)$$

If minimum disturbances are assumed at the flow entrance, the velocity at the entry port (i.e. $x=0$) can be assumed a constant over the cross section (refer Figure 3.18). The no slip condition however requires that the flow velocity is zero at the fluid-tube wall interface.
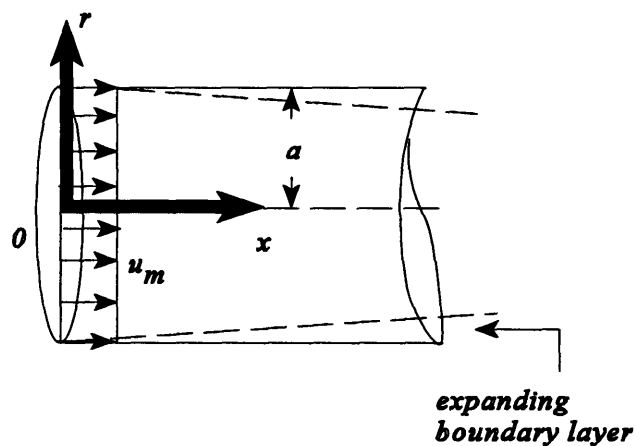

Figure 3.18 Schematic of the flow conditions assumed at a circular tube inlet. The velocity u_m represents the average flow velocity.

This results in the formation of a boundary layer which can be assumed infinitesimally thin at the entrance (equivalent to the assumption of a constant flow velocity over the entry cross sectional area) but growing over the tube length until its thickness becomes equal to the tube radius a (refer Figure 3.18). This characteristic length over which this occurs is termed the entry length, and will be discussed in more detail subsequently. Given the preceding constraints, the following boundary conditions

can now be defined:

$$u = u_m \quad \text{and} \quad v = 0 \qquad \text{at} \qquad x = o,$$

$$u = o \quad \text{and} \quad v = 0 \qquad \text{at} \qquad r = a$$

with u_m representing the average axial flow velocity. Atkinson and Goldstein have solved the preceding set of equations to relate the function $\Delta p/(1/2\rho u_m^2)$ to the function x/aR_e (with x representing the distance over which the pressure drop Δp is considered). Their calculated values of $\Delta p/(1/2\rho u_m^2)$ for varying x/aR_e are shown in both a tabulated and graphical form below.

x/aR_e	$\Delta p/(1/2\rho u_m^2)$	x/aR_e	$\Delta p/(1/2\rho u_m^2)$	x/aR_e	$\Delta p/(1/2\rho u_m^2)$	x/aR_e	$\Delta p/(1/2\rho u_m^2)$
0	0	0.009	1.00	0.030	2.1	0.10	4.59
0.001	0.32	0.011	1.11	0.040	2.51	0.11	4.92
0.002	0.46	0.013	1.22	0.05	2.88		
0.003	0.56	0.015	1.33	0.06	3.24		
0.004	0.65	0.015	1.36	0.07	3.59		
0.005	0.73	0.020	1.63	0.08	3.93		
0.007	0.87	0.025	1.88	0.09	4.26		

Table 3.4 Calculated values of $\Delta p/(1/2\rho u_m^2)$ for varying x/aR_e.
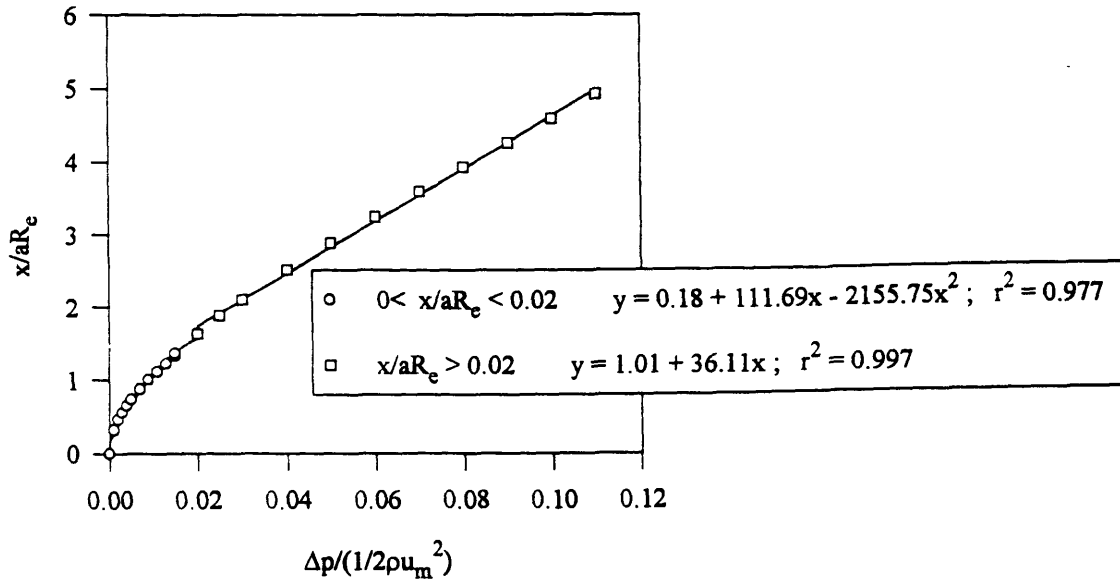
Figure 3.19 A graphical representation of the values of $\Delta p/(1/2\rho u_m^2)$ for varying x/aR_e as computed by Atkinson and Goldstein.

This information was used in computing the Reynolds number as follows: An x/aR_e value can be computed using the measured distance l between the bladder neck and distal urethral pressure measurement, and the flowrate Q. For this, the term x/aR_e can first be simplified by substituting equation (58) for the Reynolds number R_e in x/aR_e yielding:

$$\frac{x}{aR_e} = \frac{x\mu}{a\rho VD} \qquad (62)$$

Equation (62) can be further resolved by noting that $D = 2a$, and that $V = Q/\pi a^2$. Equation (62) thus now reduces to:

$$\frac{x}{aR_e} = \frac{x\mu\pi a^2}{2\rho a^2 Q} \Rightarrow \frac{x}{aR_e} = \frac{1}{2}(\frac{\pi l \nu}{Q}) \qquad (63)$$

The final form of x/aR_e as shown in equation (63), is obtained by noting that (a)

the ratio ρ/μ is defined as the kinematic viscosity v and, (b) since this thesis is concerned with characterizing the pressure drop between the bladder neck and point of distal urethral pressure measurement, $x=l$. A value of 8×10^{-7} m^2/s (corresponding to the kinematic viscosity of water at 37°C) was used to approximate the kinematic viscosity of the one-half normal saline used for bladder filling during the experimental protocol. The measured l distances are tabulated below:

Animal number	l (mm)
6	38
8	48
9	42

Table 3.5   Distance l between the bladder neck and point of distal pressure measurement for animals 6, 8 and 9.

Once an x/aR_e value was computed, the results of Atkinson and Goldstein (refer Figure 3.19 and Table 3.4) were used to compute the corresponding $\Delta p/(1/2 \rho u_m^2)$. Since both the fluid density ρ (approximated as 1000 kg/m^3) and the pressure drop Δp between the bladder neck and distal urethra are known, it is now possible to compute the average flow velocity u_m as:

$$u_m = \sqrt{\frac{\Delta p}{\frac{1}{2}\rho(\frac{l}{aR_e})}}$$
(64)

Finally, the tube (i.e. urethral) diameter D can be computed using:

$$D = \sqrt{\frac{4}{\pi}(\frac{Q}{u_m})}$$
(65)

Now, since the flow velocity V, and urethral diameter D are both known, equation (58) can be used to compute a Reynolds number. This was done, however, with the following considerations.

Ideally, the Reynolds number is used to characterize flow through a passive tube (either rigid or distensible). The electrical stimulation, by triggering a urethral contraction (as discussed in section 3.1), may thus confound the interpretation of any Reynolds number obtained during the stimulation period. Further, the applicability of the Atkinson and Goldstein formulation to an active urethra is also questionable. Hence, flow velocities, urethral diameters and Reynolds numbers were computed only during the period of zero stimulation (i.e. between the stimulation terminus and the voiding terminus). Within this window, velocities, diameters and Reynolds numbers were computed every 0.1 seconds.

Also, the Atkinson and Goldstein method used, although allowing the cross sectional area A to vary in time, at a given time instant t, assumes a uniform cross sectional area through the entire urethral length (i.e. $A=A(t)$). The urethra however is a distensible tube whose cross sectional area can vary both in time and in space (i.e. $A=A(x,t)$). By constructing its cross sectional area measure using the flowrate Q (as defined by the urethral flow controlling zone fcz - refer section 1.3.1.2), the Atkinson and Goldstein method, effectively computes an instantaneous cross sectional area value for the flow controlling zone. However, since the flow controlling zone defines urethral flow, the local cross sectional areas adjacent to the fcz are relatively unimportant to a urethral dynamics analysis. Thus, even though the Atkinson and Goldstein method considers only the fcz, it is still an extremely powerful analytical tool. When reviewing the following results, the reader should nonetheless its limitations in mind.

Due to errors incurred when computing the pressure difference between the bladder neck and point of distal urethral pressure measurement, only the results from animals 6, 8 and 9 could be used in the preceding analysis - As discussed in section 3.1.1, the p_{det}-p_{DU} pressure difference computation effectively compounds the error in a single pressure measurement. In animals 2 and 5, the resulting error yielded a negative pressure

difference, making the use of the Atkinson and Goldstein method impossible.

The peak Reynolds numbers (here, the peak number refers to the first Reynolds number obtained immediately proceeding the termination of the electrical stimulation) computed for the non-obstructed runs $Re^{p}_{non-obs}$ of all animals lay within the range 500 to 1500.

$$500 < R_{e}^{p}{}_{non-obs} < 1500$$

The Reynolds numbers were observed to decline from their peak values (to zero) as the respective voiding cycles progressed to their termination. This was expected since both the flow velocity Q and the urethral diameter D (both defining the numerator of the Reynolds number expression - refer equation (58)) monotonically decline during the same period. Given both the range of the computed Reynolds numbers and the criteria for defining laminar and turbulent flow (refer p82), it can be concluded that all urethral flows within the period of consideration were laminar. (Even if flows from the time of peak voiding flowrates are considered, the corresponding Reynolds numbers typically lay in the range of $2400 < R_{e} < 4000$. Thus, even from this vantage, only laminar and transitional flows were present, with minimal pure turbulence).

With the introduction of an outlet obstruction, the Reynolds numbers were observed to remain within the boundaries of laminar flow. These obstructive Reynolds numbers were also observed to decrease as the voiding cycle progressed. The declining flowrates and urethral diameters (as the urethra relaxes) must again be held responsible for this behavior. As discussed in section 3.1.2, the constant stimulation time holds the total contraction duration for a given animal approximately constant. As outlet obstruction was increased, the time to urethral opening t_{o} was also observed to increase (refer Figure 3.2). Hence, as outlet obstruction is increased, the time to opening t_{o} will increasingly extend into the stimulation duration (i.e. the ratio t_{o}/(stimulation duration) will increase). Given that voiding proper is defined only for times $t > t_{o}$ and that the ratio t_{o}/(stimulation duration) will vary with obstruction, the relation between the stimulation duration and the period of voiding proper must also vary according to the degree of outlet obstruction.

The point at which stimulation terminates in a voiding cycle, therefore, must also vary with obstruction. Since this point of stimulation termination effectively defines the peak Reynolds number R_e^p for a voiding cycle, it is difficult to make any meaningful comparisons between the peak Reynolds numbers under non-obstructive and obstructive conditions. The computed peak Reynolds numbers with the corresponding diameters are tabulated below.

Dog 6			Dog 8			Dog 9		
% cuff volume	R_e^p	diameter (mm)	% cuff volume	R_e^p	diameter (mm)	% cuff volume	R_e^p	diameter (mm)
0	821	1.74	0	1491	2.35	0	541	1.76
61.5	681	0.89	18.2	1472	1.77	37.5	702	1.27
76.9	707	0.75	27.2	1501	1.73	50.0	257	0.81
84.6	688	0.77	36.4	1648	1.77	62.5	562	0.78
92.3	834	0.57	45.5	1519	1.69	75.0	528	0.70
61.5	819	1.14	54.5	1488	1.49	87.5	331	0.50
69.2	1274	1.25	63.6	1220	1.33			
			72.7	1248	1.11			
			81.8	938	0.91			
			90.9	611	0.69			

Table 3.6   Summary of the computed peak Reynolds numbers with the corresponding urethral flow controlling zone diameters.

As discussed previously, the Atkinson and Goldstein method effectively considers only the urethral flow controlling zone *fcz*. The diameters emerging from this method thus characterize the *fcz* diameter as outlet obstruction is varied. Since the sphincter cuff

functions as an outlet obstruction, it effectively defines an *fcz* in its underlying urethra at each cuff volume (refer section 1.3.1.2). Also, since the cuff will constrain its underlying urethra (and thus, the effective *fcz*) to successively smaller fully relaxed diameters as the cuff is inflated (i.e. as outlet obstruction is increased) one can expect the computed *fcz* diameter to decrease as outlet obstruction is increased. This is qualitatively seen in the results presented in Table 3.5 (especially in animals 8 and 9).

Representative diagrams of the Reynolds number trends under obstructive and non-obstructive conditions, for animals 6, 8 and 9 are presented in Figures 3.20, 3.21 and 3.22.
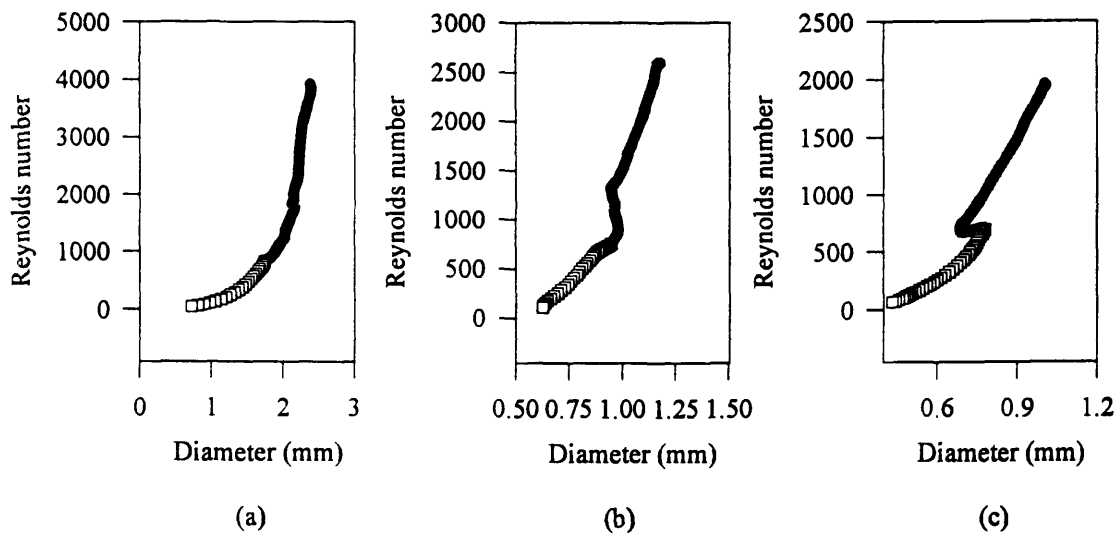

(a)   (b)   (c)

Figure 3.20 The computed Reynolds numbers for animal #6. Each curve represents the voiding period between peak flow and voiding terminus (i.e. t_{pas}) for the specific cycle. The times of stimulated and non-stimulated voiding within this period are represented by the closed circles and open squares respectively. Figure 3.20a shows values obtained under non-obstructive conditions. Figures 3.20b and c represent Reynolds numbers obtained for a 61.5% and 84.6% outlet obstruction respectively.
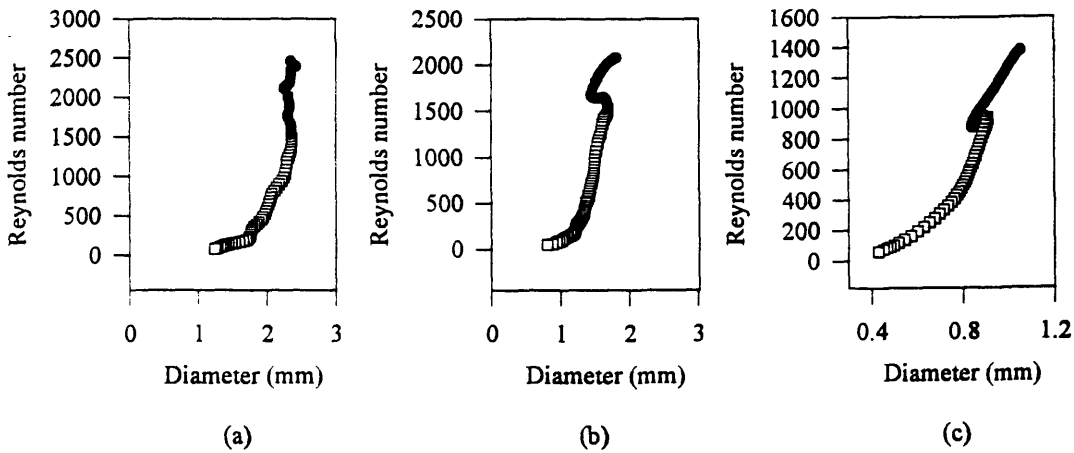
Figure 3.21   The computed Reynolds numbers for animal #8. Each curve represents the voiding period between peak flow and voiding terminus (i.e. t_{pas}) for the specific cycle. The times of stimulated and non-stimulated voiding within this period are represented by the closed circles and open squares respectively. Figure 3.21a shows values obtained under non-obstructive conditions. Figures 3.21b and c represent Reynolds numbers obtained for a 63.6% and 81.8% outlet obstruction respectively.
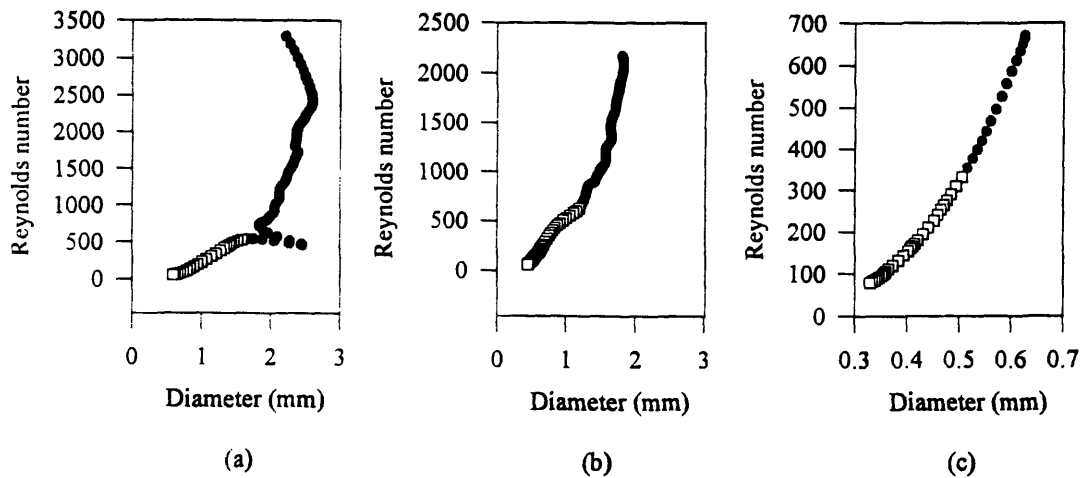

Figure 3.22   The computed Reynolds numbers for animal #9. Figure 3.22a shows values obtained under non-obstructive conditions. Each curve represents the voiding period between peak flow and voiding terminus (i.e. t_{pas}) for the specific cycle. The times of stimulated and non-stimulated voiding within this period are represented by the closed circles and open squares respectively. Figures 3.22b and c represent Reynolds numbers obtained for a 62.5% and 87.5% outlet obstruction respectively.

The urethral areas computed using the Atkinson and Goldstein method can also be used to generate a urethral tube law in terms of a detrusor pressure p_{det} vs. urethral cross sectional area A relation. The tube laws derived under obstructive and non-obstructive conditions for animals 6, 8 and 9 are presented in Figures 3.23, 3.24 and 3.25.

The instantaneous slopes along the tube law curve are representative of the instantaneous urethral contractility (or equivalently, the inverse of the instantaneous urethral compliance) as indicated below. Here, the urethra has been approximated to a cylindrical tube of constant length l and cross sectional area A.

$$Compliance = \frac{dV}{dp} = \frac{dlA}{dp} = \frac{ldA}{dp} \qquad (66)$$

Figure 3.23   Tube laws for animal #6. The solid circles represent the tube law computed under non-obstructive conditions. All open symbols denote tube laws under varied outlet obstructions.

Detrusor pressure p_{det} (cmH$_2$O)

Urethral cross-sectional area (mm^2)

- non-obstructed
- ▲ 18.2% isometric cuff volume
- □ 27.2% isometric cuff volume
- ▼ 36.4% isometric cuff volume
- ◇ 45.5% isometric cuff volume
- ○ 54.5% isometric cuff volume
- ○ 63.6% isometric cuff volume
- ▲ 72.7% isometric cuff volume
- ⊕ 81.8% isometric cuff volume
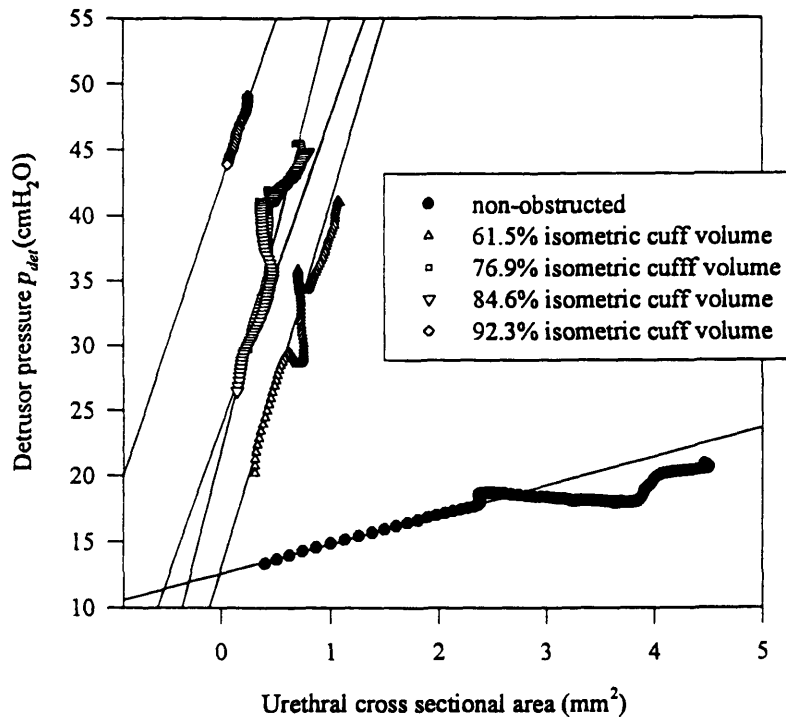- ⊡ 90.9% isometric cuff volume

Figure 3.24   Tube laws for animal #8. The solid circles represent the tube law computed under non-obstructive conditions. All open symbols denote tube laws under varied outlet obstructions.

Detrusor pressure p_{det} (cmH$_2$O)

Urethral cross sectional area (mm^2)

- non-obstructed
- △ 37.5% isometric cuff volume
- □ 50% isometric cuff volume
- ▽ 62.5% isometric cuff volume
- ◇ 75% isometric cuff volume
- ○ 87.5% isometric cuff volume

Figure 3.25   Tube laws for animal #9. The solid circles represent the tube law computed under non-obstructive conditions. All open symbols denote tube laws under varied outlet obstructions.
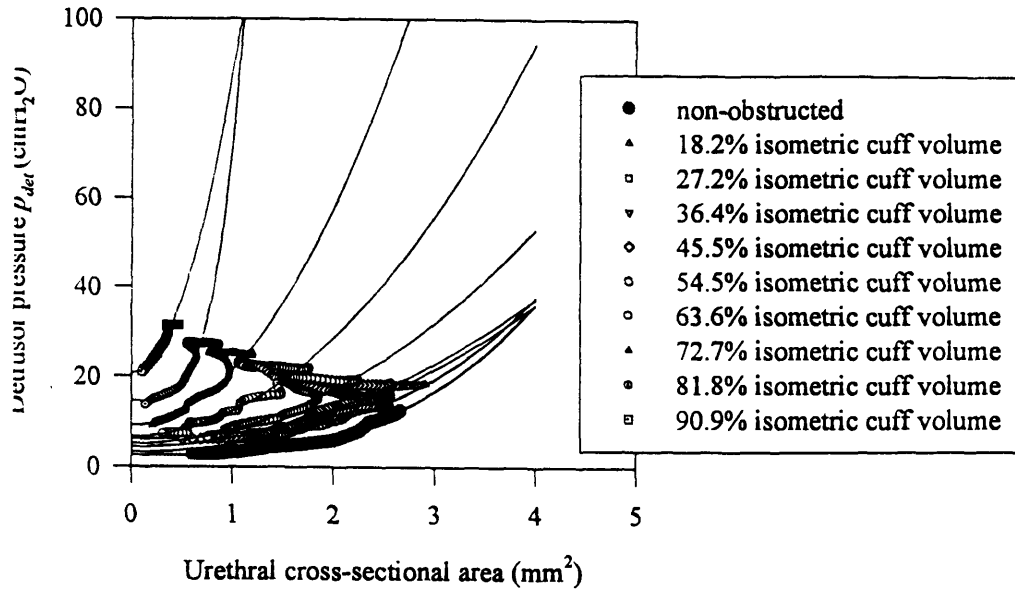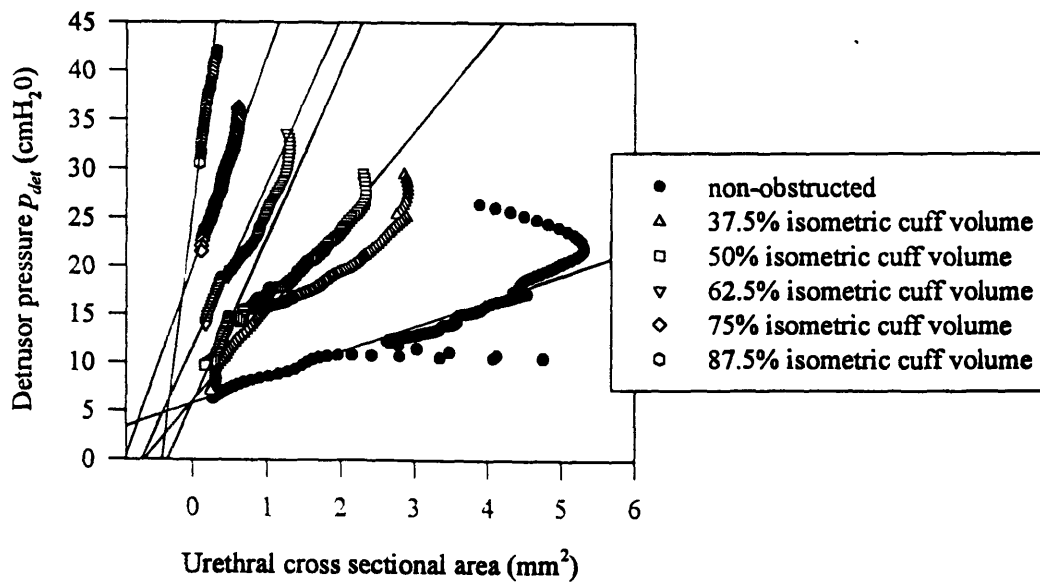
Since the instantaneous slope of the tube law is dp/dA,

$$\frac{dp}{dA} = \frac{1}{compliance} = \frac{1}{(dv/dp)}$$ (67)

An inverse relation between the urethral compliance and the urethral contractility can also be postulated as discussed for the bladder in equation (39). The reader is reminded that the Atkinson and Goldstein method used to compute the tube law, as addressed in section 3.2.1.1, computes the cross sectional area of the flow controlling zone. Hence, the preceding tube laws specifically represent the pressure-area relation of the flow controlling zone *fcz*. Equations (66) and (67) are still valid in this context if one now assumes that the flow controlling zone is modeled by the cylinder of length *l* and cross sectional area *A*.

When comparing Figure 3.23, 3.24 and 3.25, it can be seen that some tube laws are linear while others show a polynomial relation. It is our belief that all urethrae analyzed possessed some polynomial pressure-area relation (as characteristic of distensible tubes), but that the electrical stimulation used to initiate a detrusor contraction masked this when the total contraction time was small relative to the stimulation duration. Here, as discussed in section 3.1.2, the total contraction duration was observed to vary among animals, even though a constant stimulation time was maintained during all functional analyses (with the constant stimulation time holding all contraction durations for a given animal approximately constant). This variation in the total contraction durations coupled to the constant stimulation time implies that the voiding point corresponding to the instant of stimulation termination will not be uniform across all animals. Hence, in those animals with a relatively short contraction duration, as with animal 6, the stimulation will continue far into the voiding cycle leaving only a small linear region representative of zero stimulation (i.e. a pure urethral relaxation)[i]. Conversely, in animals with relatively longer

---

[i] The reader is reminded that the Atkinson and Goldstein method used to compute the urethral cross sectional areas and diameters was used to only characterize voiding from the stimulation terminus to voiding terminus.

contraction durations, the same stimulation will allow a longer period of pure urethral relaxation, producing the polynomial tube law.

A comparison of the tube laws also indicate that the compliance of the flow controlling zone decreases (i.e. the slope of the tube law increases) as the severity of the outlet obstruction is increased. This can be explained by considering the behavior of the sphincter cuff as its internal volume is increased. Here, as the cuff is inflated, it constrains the underlying urethral wall, effectively stiffening it and reducing its compliance. (Further, as discussed in section 1.3.1.2 and shown in Figure 1.14, as the cuff is inflated and an outlet obstruction is created, the flow controlling zone will move from its normal anatomical location to the urethral region immediately underlying the cuff).

3.2.2   Developing and fully developed flow in tubes

Given laminar flow in a tube of radius a and a mean axial velocity u_m, a parabolic velocity profile with the axial velocity u varying as,

$$u(r)=2u_m(1-\frac{r^2}{a^2}) \qquad (68)$$

(where r refers to the radial distance from the tube axis) is described in the literature. However, this parabolic profile does not emerge at the tube inlet itself. Rather, it requires a characteristic tube length termed the entrance (or, entry) length to fully develop its parabolic characteristic. Flow within the entrance length is termed entry length or developing flow, while flow in tube segments proceeding the entry length is termed fully developed flow. Developing and fully developed flows exhibit different characteristics, and will be briefly discussed below. The reader is referred to the numerous excellent Fluid Mechanics texts available such as the Gerhart and Gross of references (14) and (15), if additional information is required. Fully developed flows are often assumed in

fluid mechanics analyses because they are relatively easier to assess in that they are unidimensional and unidirectional.

As described briefly in section 3.2.1.1, if a fluid enters a tube with minimum disturbances, the velocity at the inlet port can be assumed approximately uniform over the entrance cross section. Nonetheless, the no slip condition requires that at the tube wall, the flow velocity is zero. Hence, one can imagine a layer of slower moving fluid around the tube wall (whose motion is retarded by the wall shear stresses), beginning at the entry port with infinitesimal thickness and gradually growing in the direction of flow. This layer of slower moving fluid is termed a boundary layer, and its growth in the axial direction is fueled by the radial propagation of wall shear stresses. The effects viscosity and rotation (i.e. shear stresses and turbulence) are limited to the boundary flow (as postulated in Prandtl's boundary layer hypothesis).
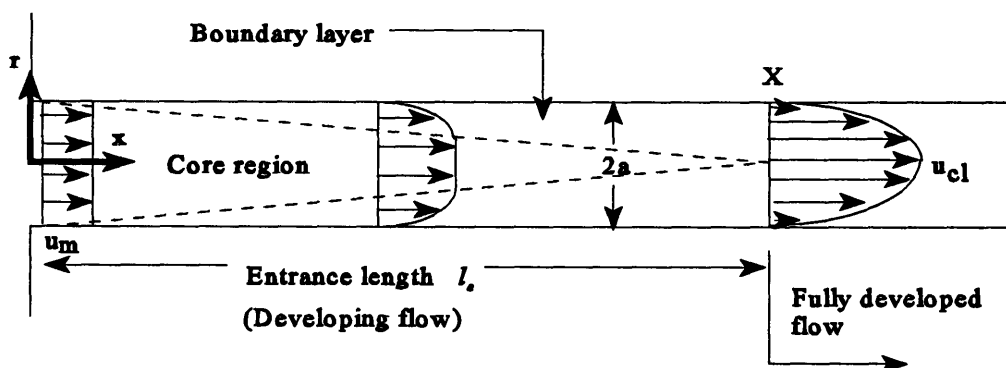

Figure 3.26 Schematic of the entrance length, entry length (developing) flow and fully developed flow in a tube. u_m denotes the average flow velocity, while u_{cl} represents the centerline flow velocity.

Therefore, within the envelope of the boundary layer, one can also imagine a core of ideal fluid with a zero viscosity and turbulence. The boundary layer thickness itself will increase until it is equal to the tube radius. At this point, the margins of the boundary layer have effectively fused along the tube axis (refer Figure 3.26), and thus distribute the

effects of viscosity (and turbulence, if present) through the entire tube cross sectional area.

Since fully developed flow begins only after the thickness of the boundary layer is equal to the tube radius (point X in Figure 3.26), the entrance length can alternately be described as the tube length required for the fusion of the boundary layer free margins. It is shown in Figure 3.26 that the centerline flow velocity u_{cl} (defined as the flow velocity at the tube axis, i.e. $r=0$) increases during developing flow. This occurs because as the peripheral fluid layers become retarded by the wall shear stresses, fluid in the central core accelerates to maintain a constant flowrate (required by the conservation of mass for an incompressible fluid flowing through a tube of constant cross sectional area A - refer equation (5)). Once fully developed conditions are attained, the centerline velocity remains a constant at $u_{cl} = 2\ u_m$ (refer equation (68), with $r=0$).

The pressure gradient in the axial direction also varies depending on whether developing or fully developed conditions are attained. This is schematically shown in Figure 3.27.
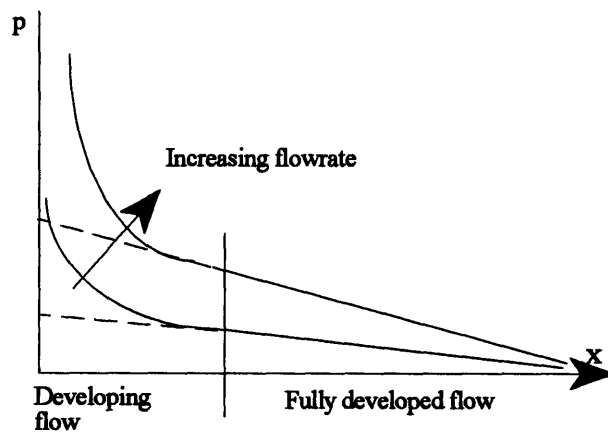

Figure 3.27   Schematic of the pressure drop along a tube with flow changing from entry length to fully developed conditions.

The steeper gradient of pressure decrease in the developing region is due to the presence of both an increased convective pressure drop (defined as $1/2\rho v^2$ - refer section

1.3.1.2) due to the acceleration of the central fluid core, and higher wall shear stresses.

One can use dimensional analysis to determine that the ratio of the entrance length l_e to the tube diameter D ($D=2a$ - refer Figure 3.26) is a function of the Reynolds number R_e. Thus,

$$\frac{l_e}{D} = F(R_e) \qquad (69)$$

The exact functional expression of F has been determined analytically, and is given below. It should be noted that F differs in laminar and turbulent flow, and that in turbulent flow, the entry length l_e exhibits small dependence on the Reynolds number R_e.

$$l_e/D \approx 0.06R_e \qquad \text{Laminar flow} \qquad (70)$$

$$l_e/D \approx 4.4R_e^{1/6} \qquad \text{Turbulent flow} \qquad (71)$$

Typically, the peak urethral diameters D computed (corresponding to the point of peak Reynolds number R_e^P) lay in the range of 1.5mm $<D<$ 2.5mm (Refer Table 3.6). Given these values, and the range of Reynolds numbers computed, it is possible to estimate an entrance length for the urethra.   Since it has been established that all urethral flows analyzed were laminar, the entry lengths corresponding to the peak Reynolds numbers l_e^P can be computed by substituting the peak Reynolds number and corresponding diameter value form each animal into equation (70) yielding,

$$l_e^P = 0.06(821)(1.72) = 85.71mm \qquad \text{for animal 6}$$

$$l_e^P = 0.06(1491)(2.35) = 210.23mm \qquad \text{for animal 8}$$

$$l_e^P = 0.06(541)(1.76) = 57.12mm \qquad \text{for animal 9}$$

The total urethral length l_T is computed from the sum of the lengths from bladder neck to the point of distal urethral pressure measurement l and the length from the point of distal urethral pressure measurement to the external meatus l',

$$l_T = l + l' \qquad (72)$$

The relevant l values have already been presented in Table 3.5. They are repeated in Table 3.7 along with their corresponding l' and total urethral lengths.

Animal	l (mm)	l' (mm)	l_T (mm)	l_e
6	38	50	88	85.71
8	48	42	90	210.23
9	42	35	77	57.12

Table 3.7   Summary of the relevant urethral length parameters used in the estimation of a total urethral length with their corresponding entrance lengths.

From the results in Table 3.7, one can conclude that typically, urethral flows at relatively high flowrates are entry length flows with fully developed conditions forming (if at all) proximal to the external meatus. Since it is established that both Reynolds numbers and fcz diameters decrease as a voiding cycle progresses towards its termination (refer Figures 3.20, 3.21 and 3.22), one can also use equation (70) to predict that the probability of attaining fully developed conditions in the entire urethra will increase as a voiding cycle progresses to its termination (as the Reynolds numbers and fcz diameters fall, the corresponding entry lengths will also reduce to $\leq$ the total urethral length l_T).

4 Conclusions

The canine model of the human urinary tract is consistent in that the computed passive outlet resistance increased as outlet obstruction was increased. However, this increase in resistance is non-linear (Figure 3.1), indicating that the sphincter cuff is suitable to model only the upper and lower extremes of outlet obstruction. The canine model, as used, therefore, is inappropriate to model any chronic obstruction that will gradually progress from mild to moderate to severe.

The canine model shows that as outlet obstruction is increased, the peak voiding pressures p_{max} and the time to urethral opening t_o increase, while the peak voiding flowrates Q_{max} decrease, and the time to peak flow t_{Qmax} remains approximately constant. Clinically, with outlet obstruction, peak voiding pressures and both time to opening t_o and

time to peak flow t_{Qmax} are observed to increase, while peak voiding flowrates are observed to decrease. As described in section 3.1.2., the discrepancy in the clinical and experimental t_{Qmax} behavior appears to be an artifact of the stimulation process. Given the overall correspondence between the clinical observations and the experimental results, the canine model appears well suited to model the physiologic consequences of an outlet obstruction in humans.

The correlations between the internal work (as formulated by Schäfer) and the outlet resistance (Figure 3.15), and the external work and the outlet resistance (Figure 3.16) show that at low levels of outlet obstruction, both the internal work and the external work increase at a greater rate than the outlet resistance. At present, outlet obstructions are clinically assessed using an outlet resistance measure alone. Since the experimental data indicate that the internal/external work parameters are better suited to monitor the progression of mild/asymptomatic BPH, the internal and external work should at least be considered in conjunction with the outlet resistance in these patients. Similarly, the experimental data implies that an unchanging or slowly increasing outlet resistance can no longer be construed as evidence of a stable outlet obstruction unless corroborated by a static internal work or external work level. The reader is again reminded that the internal work parameter discussed here assumes a perfectly elastic bladder at all times, and is thus not a physiologically reasonable construct. However, even with its limitations, this concept of internal work is an effective prognosticator of outlet obstruction. Unlike the internal work, the formulation of the external work involves no physiologic caveats. A changing external work must thus be considered a prime indicator of a changing outlet obstruction.

At moderate levels of obstruction, the distinction (in terms of a sensitivity to a changing outlet obstruction) between the work and resistance parameters begins to wane, as the rates of increase of the internal and external work begin to plateau and approximate the rate of increase of the outlet resistance. In fact, at high enough obstructions, the experimental data show that both the internal work and the external work saturate, leaving the outlet resistance as the sole indicator of any further change in outlet obstruction. At

moderate/severe obstructions, therefore, the present practice of evaluating only the outlet resistance appears adequate.

Figure 3.12 shows that the total detrusor work increases as outlet obstruction is increased. This total work response is divided into its internal and external work components in Figure 3.13. Here, it is seen that at low outlet obstructions, the magnitudes of the detrusor internal work and external work are approximately equal. One could argue that this is evidence for the simple voltage source and capacitor model (with no intrinsic resistance), where the detrusor internal work is fully recovered during the period of voiding proper. However, the model including the effects of fatigue also predicts this behavior if it assumed that during non/minimal obstructive conditions the contracting detrusor does not fatigue (the reader is reminded that this model predicts a difference between the energy available to drive flow at a given detrusor pressure, and the work required to reach that pressure only if the detrusor has fatigued). As outlet obstruction is increased, the data show that the internal work begins to increase rapidly, while the external work gradually decreases. Thus, at high outlet obstructions, successively larger proportions of the work done to elevate the detrusor pressure p_{det} above a critical opening pressure p_{cuo} cannot be recovered. This, while effectively invalidating the simple non-fatiguing detrusor model, is consistent with a detrusor gradually fatiguing while attempting to drive flow against an increasing outlet obstruction, with the increased "dissipation" (i.e. fatigue) accounting for the discrepancy between the internal and the external work. At a completely isometric contraction, the detrusor external work is zero. Here, one can use the elastic internal work formulation of $W=V\Delta p$ (with the Δp representing the pressure difference between the peak isometric pressure and the baseline pressure) as a first approximation of the maximum energy available to drive a urethral flow.

The increase in the total detrusor work with increasing outlet obstruction is also consistent with the notion of a detrusor with a limited ATP energy store. Here, one can imagine successively larger fractions of a fixed ATP store being exhausted in driving flows against an increasing obstruction, until the total available ATP is insufficient to increase

the detrusor pressure above some critical p_{cuo} (at which point the total work will equal the "internal work").

       The computed Reynolds numbers indicate that all flows considered were laminar, while the computed entry lengths (when compared to the corresponding total urethral lengths) show that urethral flows are typically entry length flows with the possibility of fully developed flow occurring only proximal to the external meatus. This concept of a predominantly entry length laminar flow is consistent with the PURR assumption of a quadratic relation between the detrusor pressure and flowrate. (If the flow was fully developed laminar flow, then the detrusor pressure must be linearly proportional to the flowrate as defined by the Poiseuille equation. A quadratic relation can, however, exist with laminar entry length flow since the pressure gradient along the entry length is non-linear, refer Figure 3.27). The Atkinson and Goldstein model used to compute the Reynolds numbers and urethral areas is consistent in that the resulting urethral areas increase with increasing pressures and Reynolds numbers (i.e. flowrates). The tube laws are also consistent in that the urethral (i.e. the urethral flow controlling zone) compliance decreases as the outlet obstruction is increased.

5 Bibliography

1.   Gleason, D.M., Bottaccini, M.R., Drach, G.W. Urodynamics. *Journal Urol.* 115:356-361, 1976.

2.   Griffiths, D.J. Mechanics of Micturition, *Neurology and Urodynamics, Principles and Practice.* S.V.Yalla, E.J.McGuire, A.Elbadawi, J.G.Blaivas (Ed). McMillan Publishing Company, New York. 1988, pp 96-105.

3.   Smith, J.L., Cravalho, E.G., *Engineering Thermodynamics.* pp 350 -358.

4.   Griffiths, D.J., Hydrodynamics and Mechanics of the Bladder and Urethra, *Urodynamics, Principles, Practice and Application.* A.R. Mundy, T.P. Stephenson, A.J. Wein, (Ed), Churchill Livingstone, Edinburgh, London, Melbourne, and New York, 1984.

5.   Schafer, W. Detrusor as the Energy Source of Micturition. *Benign Prostatic Hyperplasia.*F. Hinman Jr. (Ed). p 451.

6.   Sullivan, M.P., DuBeau, C.E., Resnick, N.M., Cravalho, E.G., Yalla, S.V., Abinitio Continuous Occlusion Test to Determine Detrusor Contractile Performance, *Journal of Urology,* in press.

7.   Yalla, S.V., Merit Review Proposal.

8.   Yalla, S.V., Badawy, H, Radiologic and Urodynamic Abnormalities in Spinal Chord Diseases. H. Pollack (Ed), *Clinical Urography.* W.B.Saunders Co, Philadelphia, 1989.

9.   Fowler, F.J., Wennberg, J.E., Timothy, R.P., Barry, M.J., Mulley, A.G., Hanley, D. Symptom Status and Quality of Life Following Prostatectomy. *JAMA.* 259: 3019-3022,   1988.

10. Malone, P.R., Cook, A., Edmonson, R., Gill, M.W., Shearer, R.J. Prostatectomy, Patients' Perception and Long-Term Follow-Up. *Brit. J. Urol.* 61: 234-238, 1988.

11. Sibley, G.N.A. An Experimental Model of Detrusor Instability in the Obstructed Pig. *Brit. J. Urol.* 57: 292-298, 1988.

12   Dixon, J.S., Gilpin, C.J., Gilpin, S.A., Gosling, J.A., Brading, A.F., Speckman, M.J. Sequential Morphological Changes in the Pig Detrusor Response to Clinical Partial Urethral Obstruction. *Brit. J. Urol.* 64: 385-390, 1989.

13. Schäfer, W., Fischer, B., Meyhoff, H.H., Lutzeyer, W: Urethral resistance during voiding: I. The passive urethral resistance relation, PURR. II. The dynamic urethral resistance relation, DURR. Proceedings of the XIth Annual Meeting of the International Continence Society, Leiden, 1982.

14. Gerhart, P.H., Gross, J.R., *Fundamentals of Fluid Mechanics*, Addison-Wesley Publishing Co. 1985, pp 160-161.

15. Gerhart, P.H., Gross, J.R., *Fundamentals of Fluid Mechanics*, Addison-Wesley Publishing Co. 1985, p 405.

16. *Modern Developments in Fluid Dynamics*, Vol. II, S. Goldstein (Ed), Dover publications, New York, 1965, pp 299-309